Optical conductance fluctuations: Diagrammatic analysis in the Landauer approach and nonuniversal effects

M. C. W. van Rossum,[1] Th. M. Nieuwenhuizen,[1] and R. Vlaming[2]
[1] *Van der Waals-Zeeman Laboratorium, Universiteit van Amsterdam, Valckenierstraat 65, 1018 XE Amsterdam, The Netherlands*
[2] *Instituut Theoretische Fysica, Universiteit van Amsterdam, Valckenierstraat 65, 1018 XE Amsterdam, The Netherlands*
(Received 30 November 1994)

The optical conductance of a multiple scattering medium is defined as the total transmitted light of a normalized diffuse incoming beam. This quantity, analogous to electronic conductance, exhibits universal conductance fluctuations. We perform a detailed diagrammatic analysis of these fluctuations. With a Kadanoff-Baym technique all the leading diagrams are systematically generated. A cancellation of the short distance divergencies occurs that yields a well behaved theory. The analytical form of the fluctuations is calculated and the theory is applied to optical systems. Absorption and internal reflections, which are taken into account, reduce the fluctuations significantly.

PACS number(s): 42.25.Bs, 72.20.-i,78.20.Dj

I. INTRODUCTION

When studying the transmission of optical waves through random media one may consider fluctuations in the *optical conductance*. Analogous to the electronic conductance, this quantity is obtained when, first, the incoming beam is monochromatic and diffuse, and, second, all outgoing light is collected. Since the electronic conductance is known to exhibit so called universal conductance fluctuations (UCF), the same fluctuations are expected in the optical conductance. Measurements of this quantity would constitute a cornerstone in the analogy between optical and electronic mesoscopic systems.

We briefly review the situation for mesoscopic electron systems [1–5]. The electronic conductance of mesoscopic samples is known to show reproducible sample to sample fluctuations. Since the fluctuations are a consequence of scattering from static impurities, they are static. Their magnitude is independent of the sample parameters, such as the mean free path, the sample thickness, and the average conductance. Hence they are called universal conductance fluctuations. The mean conductance in the considered regime comes from multiple scattered diffuse electrons. The UCF are a consequence of interference of multiple scattered waves, causing correlations between two diffuse paths. Therefore the fluctuations are much larger then one would obtain classically by modeling the system by a random resistor array, in which interference effects are neglected. That approach is valid only on a length scale exceeding the phase coherence length, where the fluctuations reduce to their classical value. The conductance fluctuates when the phases of the waves in the dominant paths are changed. This happens, of course, if one changes the position of the scatterers, e.g., by taking another sample. One may also keep the scatterers fixed but apply a magnetic field or vary the Fermi energy. (In an optical system one can vary the frequency of the light.) In all these cases one modifies the phases of scattered waves, so that different propagation paths become dominant.

Transport through mesoscopic systems is studied not only in electron systems, but also using multiple scattered classical waves such as sound, microwaves, and, particularly, light. The origin of the mesoscopic phenomena is the interference of multiple scattered waves and in first approximation all systems are described by the same equations, namely, the scalar wave equation; see, for instance, Ref. [6] for a review. Thus one expects that similar large fluctuations in optical systems are present in the diffuse transmission regime. An advantage of optical systems over electronic ones is that optical systems are much cleaner: no equivalents of phonons or electron-electron interactions are present. Indeed, very accurate measurements of the enhanced backscatter cone [7], correlation functions [8,9], and intensity distributions [10] were performed. Nevertheless, to the best of our knowledge, the optical analog of the UCF has not yet been observed in optical systems. Such experiments turn out to be difficult. Although the magnitude of the fluctuations is universal, they occur on a background of order g, where g is the dimensionless conductance (in optical experiments one typically has $g \sim 10^3$). The relative value of the fluctuations to the background is thus $1/g$, so that the C_3 correlation function is of order $1/g^2$, typically of order 10^{-6}. For electrons this problem is absent as moderate values of g are achievable. This is also the reason that electrons are more easily brought near Anderson localization, for which g has to take a critical value of order unity. In the electronic case the moderate values of g, combined with very sensitive techniques for current measurements, have led to many observations of the universal conductance fluctuations. Recent optical experiments suggest, however, that the optical analog of UCF should just be experimentally accessible, as the measurement of the third cumulant in the total transmission was reported [10]. This quantity is of the same order as the

optical UCF, namely $1/g^2$. It is expected that similar techniques can be applied to measure the optical UCF. Microwave scattering is also interesting as it combines lower values of g with many of the advantages of optical systems.

We are interested not only in just the size of the fluctuations, but also in the somewhat more general frequency correlation. A change in the frequency alters the interference pattern, just as occurs by changing the magnetic field or the Fermi energy in the electronic case. It is known from experiments that using the frequency as a tunable parameter provides a good way for measuring the fluctuations. In contrast to electronic systems, in optical systems both angular resolved and angular integrated measurements of the transmission are possible. Therefore various transmission quantities can be measured in optical systems, each with its particular frequency correlation function. In a recent review by Berkovits and Feng [11] the different correlations and their physical interpretation are discussed extensively. Denoting the transmission from incoming channel a (wave coming in under angles θ_a, ϕ_a) to outgoing channel b (waves transmitted into angles θ_b, ϕ_b) as T_{ab}, the correlation functions can be classified as [11,12]

$$\frac{\langle T_{ab}(\omega)T_{cd}(\omega+\Delta\omega)\rangle}{\langle T_{ab}(\omega)\rangle\langle T_{cd}(\omega+\Delta\omega)\rangle} = 1 + C_1^{abcd}(\Delta\omega) + C_2^{abcd}(\Delta\omega) + C_3^{abcd}(\Delta\omega). \quad (1)$$

The unity just comes from the product of averages. The C_1 term in the correlation function is the most important one if the angular resolved transmission T_{ab} is measured. The reason is that C_1 is of order unity when both the incoming directions a and c and the outgoing directions b and d are, pairwise, close to each other. When dealing with one single monochromatic plane wave ($a = c$), C_1 describes the correlation of the bright and dark speckle pattern. Diagrammatically, C_1 is the sum of all reducible diagrams, that is to say, just like the unit contribution in Eq. (1), it is equal to the product of two averages.

If, instead of measuring light in one outgoing channel, all outgoing light is integrated, the sharply peaked and short ranged C_1 correlation function is overwhelmed. By collecting the outgoing light, the total transmission $T_a = \sum_b T_{ab}$ is measured; experimentally, this is commonly done using an integrating sphere [9]. In this setup the C_2 correlation function, which has a much smaller peak value but is long ranged, contributes for all outgoing angles and becomes dominant. Its long range character arises because, due to interference of the diffuse light paths, the outgoing amplitudes are pairwise in phase. The C_2 correlation, which still depends on the angles of the incoming beams a and c, is of order g^{-1}. The C_2 corresponds to a diagram where the two incoming diffusons interact through a Hikami vertex.

Finally, the C_3 term is dominant when the incoming beam is diffuse, and all outgoing light is collected, so that, just as in electronic systems, the conductance $g = T = \sum_{a,b} T_{ab}$ is measured. In that measurement contributions where a and c are far apart are dominant. In contrast to the previous case, now also these incoming amplitudes must be pairwise in phase. This occurs in a diagram where the two incoming diffusons interact twice, so that a loop occurs; in principle, further loop insertions to it also contribute. In spite of the fact that C_3 is of order g^{-2}, it dominates over the C_1 and C_2 terms as it has contributions for all incoming and outgoing angles.

The C_1 and C_2 correlations have been studied in detail, both experimentally [9,13,14] and theoretically [15]. It was also shown in experiments [16] and in theory [17,18] that absorption and internal reflection, neglected in the earliest calculations, significantly reduce the correlations. Among other methods, the C_1 and C_2 correlations were successfully [15,18] calculated using a diagrammatic technique based on the Landauer approach [19,20]. One might hope that the calculation of the C_3 or UCF in this approach is also straightforward. It is well known, however, that the calculation in the Landauer approach is quite cumbersome, since divergencies show up on scales of one mean free path when the problem is treated on a macroscopic level using diffusons.

In order to circumvent these difficulties, one is tempted to use the Kubo approach, often used in electronic systems to calculate the UCF [2–4]. Furthermore, the results for the conductance obtained by Kubo or Landauer formalism should be identical [21,22]. Yet the Kubo approach cannot be applied directly to optical systems, since it is not clear how external lines should replace current vertices, and how absorption and internal reflections are to be included. Therefore we use the Landauer approach.

Technically, the difficulties in the Landauer approach are caused by the vertices for partner exchange of two diffusons, the so called Hikami boxes. Each Hikami box brings the square of the internal momentum, whereas the current vertices are momentum independent in the Kubo formula. As a result, the integral over the internal momentum of the closed loop is convergent in the Kubo formula, while naively divergent in the Landauer approach.

Two studies of C_3 in the Landauer approach are known to us. In the first, Kane, Serota, and Lee [23] consider electronic systems and make elegant use of current conservation to derive an expression for the correlation function. Although in optical systems the conserved quantity is not the intensity but the energy, their prediction applies to optical systems as well, since it amounts to a result for the same sums of scattering diagrams, involving different parameters only. This result has not been confirmed by a direct derivation, however. Moreover, since it relies on a conservation law, it is not clear what happens when absorption is present. The second study was performed by Berkovits and Feng [11]. After giving a very clear discussion of the problem, these authors calculated one of the macroscopic diagrams (presented earlier by Feng, Kane, Lee, and Stone [12]) and subtracted the divergent parts by hand. In this way the correct order of magnitude and the qualitative frequency dependence were obtained.

It is our goal to clarify the situation by calculating the optical C_3 diagrammatically. A complete analysis of all

leading diagrams is needed, in which finally the divergent parts should cancel. We specialize to the case where the conductance is measured. In this setup the amplitudes of the incoming and outgoing diffusons are exactly in phase. If the C_3 correlation is measured as a (small) part of the correlation in the angular transmission or total transmission, this phase condition need not be fulfilled. Other contributions of order $1/g^2$ which are angular dependent are then present. These contributions are both the diagrams presented below, with different decay rates for the incoming and outgoing diffusons, but also new diagrams contribute. In conductance measurements these complications do not occur. Our fundamental approach immediately allows for inclusion of effects due to boundary layers and absorption. Our calculations, although specialized to optical systems, are valid for any mesoscopic system.

Tacitly we assumed that higher order correlations can be neglected. Altshuler *et al.* [24] have shown that for small n the nth cumulants scale as g^{2-n}, so that for $g \gg 1$ the fluctuations have indeed a Gaussian distribution; the far tail of the distribution is predicted to be log normal. It would be interesting, however, to determine the full distribution function of the fluctuations, as was done in experiment for the angular resolved transmission [13] and the total transmission [10], and recently in theoretical work by Nieuwenhuizen and Van Rossum [25].

The outline of this paper is as follows. First, we introduce the basics of the diagrammatic technique and describe diffuse transport of light. In Sec. III we present the long distance diagrams and analyze the divergencies arising from these diagrams in the diffusion approximation in Sec. IV. Next, in Sec. V we develop a Kadanoff-Baym theory in order to generate all relevant scattering diagrams. In Sec. VI we show that the divergencies indeed cancel if all diagrams are analyzed in detail. The general form of the fluctuations is calculated in Sec. VII and applied to optical systems, where absorption and internal reflections may be present. The presentation is closed with a discussion.

II. DIFFUSE TRANSPORT OF LIGHT

In this section we discuss standard aspects of diffuse light transport, such as the amplitude Green's function, the diffuse intensity, and the transport equation. We shall consider the situation of point scatterers in a medium that has a dielectric constant different from its surroundings. We employ the notation and results of the paper by Nieuwenhuizen and Luck [26]. The main results of the present section are the expression (37) for the C_3 correlation function, and the expression (39) for the universal conductance fluctuations. These expressions involve diagrams with incoming total-flux diffusons $\mathcal{L}_{\rm in}$ defined in (18), outgoing total-flux diffusons $\mathcal{L}_{\rm out}$ defined in (26), and internal diffusons $\mathcal{L}_{\rm int}$ defined in (35) or (36). Readers not interested in the microscopic background of these relations may skip the details of the present section.

We consider a quasi-one-, quasi-two-, or three-dimensional slab of thickness L and area $A = W^{d-1}$, with $W \gg L$, which contains static, isotropic point scatterers. As usual a scalar approximation is made for the electromagnetic field of the light [27]. For bulk properties this is justified since the polarization is scrambled after a few scattering events. For other applications, such as acoustic waves and spinless electrons, the scalar property is immediate. The scalar wave equation at given frequency ω reads

$$\nabla^2\psi(r) + \frac{\omega^2}{c^2}\epsilon(r)\psi(r) = 0, \tag{2}$$

where c is the vacuum speed of light. We shall consider a medium with dielectric constant ϵ_0 and density n of small spheres with dielectric constant ϵ_2 and radius a_0, located at random positions R_i. Going to the limit of point scatterers we get

$$\epsilon(r) = \begin{cases} \epsilon_0 + \frac{4}{3}\pi a_0^3(\epsilon_2 - \epsilon_0)\sum_i \delta(r - R_i), & 0 < z < L\ , \quad \text{(3a)} \\ \epsilon_1, \quad z < 0, z > L, & \text{(3b)} \end{cases}$$

where ϵ_1 is the dielectric constant in the surrounding medium. The wave numbers in the surrounding medium and in the random medium are

$$k_1 = \frac{\omega}{c}\sqrt{\epsilon_1}, \qquad k = mk_1 \equiv \sqrt{\frac{\epsilon_0}{\epsilon_1}}k_1, \tag{4}$$

respectively. In the bulk the average retarded Green's function (amplitude Green's function) in three dimensions with momentum $\mathbf{p}$ reads

$$G(\mathbf{p}) = \left(\mathbf{p}^2 - k^2 - nt\right)^{-1}. \tag{5}$$

For small scatterers the scattering becomes isotropic with an effective strength described by the t matrix [28]

$$t = \left(\frac{1}{u} - \frac{1}{u_0} - i\frac{k}{4\pi}\right)^{-1}, \tag{6}$$

where $u = 4\pi k^2 a_0^3(\epsilon_2 - \epsilon_0)/3$ is the bare scattering strength and u_0 is an internal parameter of the point scatterer. The mean free path is defined as

$$\ell = \frac{4\pi}{nt\bar{t}}, \tag{7}$$

in which n is the scatterer density. The metallic mesoscopic regime is defined by $k\ell \gg 1$ and $\ell \ll L$. Equation (6) satisfies the optical theorem $\mathrm{Im}(t) = k\bar{t}t/4\pi a$, where a is the albedo of the scatterer. The case of no absorption, which we treat first, corresponds to $a = 1$. In electronic systems absorption does not take place, but a similar behavior arises from dephasing; in that case the phase coherence length plays the role of absorption length and, for our purpose, has to be larger than the system size.

For disordered electron systems one deals with weak s-wave scattering and the diagrammatic expansion can be carried out in second order Born approximation. In experiments on optical systems, however, efficient scattering is achieved by taking resonant scatterers and strictly one now has to calculate the full Born series [28]. In

the main part of this work we study how the cancellation of some short range contributions takes place. This we do in the second order Born approximation, where $t \approx u + iu^2k/4\pi$ and $\ell \approx 4\pi/nu^2$. Working with the full Born series would introduce a large number of extra classes of diagrams so that the total number of diagrams increases dramatically. We expect, however, that the cancellation of divergencies, when shown in the second order Born approximation, also holds if the full Born series is considered. It is widely expected and confirmed in one of our earlier papers that for static quantities the difference between the two should only be a renormalization of the mean free path in the final results [29]. We thus continue to work with the full Born series where possible. The cancellation of short range divergencies will only be shown within the second order Born approximation.

Intensity transport in transmission is dominated by ladder diagrams or diffusons. A diffuson is made up by pairing one retarded and one advanced propagator sharing the same path through the sample, as is depicted in Fig. 1.

Although the transport deep in the bulk is accurately described with the diffusion equation, the precise behavior near the (reflecting) surface has to be derived from the Schwarzschild-Milne integral equation [27]. Consider a plane wave with unit flux impinging on the sample under angle θ_a

$$\psi_a^{\rm in}(r) = \frac{1}{\sqrt{Ak_1\cos\theta_a}}\, e^{iQ_a\rho + ik_1\cos\theta_a z},\ z<0, \qquad (8)$$

where $\rho = (x, y)$ is the transversal coordinate and $Q_a = k_1 \sin\theta_a(\cos\phi_a, \sin\phi_a)$ is the two-dimensional transverse momentum of the incoming beam. Inside the slab the unscattered part of the intensity decays over one mean free path. This is described by (5) since its pole lies slightly away from the real axis, due to the imaginary part of t. The source of diffuse intensity is the first scattered intensity,

$$S_a(z) = T(\mu_a)\, nt\bar{t}\, |\psi_a^{\rm in}(r)|^2 = \frac{4\pi T(\mu_a)}{Ak_1\mu_a\ell}\, e^{-z/\ell\mu_a}, \qquad (9)$$

where $\mu_a = \cos\theta_a'$ involves the angle θ_a' of the refracted beam with respect to the z axis. The source is proportional to the intensity transmission coefficient of the boundary between the two dielectrics,

$$T(\mu) = \frac{4\mu\sqrt{\mu^2 - 1 + 1/m^2}}{[\mu + \sqrt{\mu^2 - 1 + 1/m^2}]^2}. \qquad (10)$$

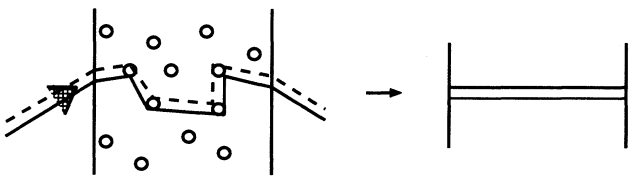

FIG. 1. Left: an example of an actual scattering process; a retarded (full line) and an advanced (dashed line) amplitude come from the left and share the same path through the sample. Right: schematic representation of the average process, the diffuson.

The twice scatterered intensity follows from S_a as $nt\bar{t}\int dr'|G(r,r')|^2 S_a(r')$. The geometric sum of first, second, third, ..., times scattered intensity is the multiple scattered or diffuse intensity $\mathcal{L}_a$. It is generated from the first scattered intensity by the Schwarzschild-Milne equation

$$\mathcal{L}_a(z) = S_a(z) + \int_0^L dz' M(z,z')\mathcal{L}_a(z'). \qquad (11)$$

The kernel M reads

$$M(z,z') = M_B(z-z') + M_L(z+z') + M_L(2L-z-z'), \qquad (12)$$

which contains the bulk term

$$M_B(z-z') = \int_0^1 \frac{d\mu}{2\mu} e^{-|z-z'|/\mu\ell}, \qquad (13)$$

and layer terms describing internal reflections at the interfaces at $z = 0$ and $z = L$. The layer term reads

$$M_L(z+z') = \int_0^1 \frac{d\mu}{2\mu}[1 - T(\mu)]e^{-(z+z')/\mu\ell}. \qquad (14)$$

It involves the total path length of the radiation going from depth z to the boundary at $z = 0$, reflected there, and going to depth z'. In the bulk of the slab (several mean free paths away from the boundaries) the diffuse intensity has a simple behavior [26],

$$\mathcal{L}_a^{\rm in}(z) = \frac{4\pi T(\mu_a)\tau_1(\mu_a)}{k_1\ell m A\mu_a}\,\frac{L + z_0 - z}{L + 2z_0}. \qquad (15)$$

Here τ_1 is a factor that determines the limit intensity of a semi-infinite slab; of course, it depends on the incident angle. The length z_0 is called the "injection depth." For isotropic scattering one has [27] $z_0 = 0.7104\ell$. However, it becomes larger when there is a mismatch of the indices of refraction between the scattering medium and the surroundings [28]. Note that (15) satisfies the diffusion equation $\nabla^2\mathcal{L}_a^{\rm in} = 0$; the more complicated Schwarzschild-Milne equation is needed to fix the parameters of its solution.

In the electronic conductance measurements, however, waves coming from all directions are involved. In the Landauer formula for the conductance,

$$G = \frac{2e^2}{h}\sum_{ab} T_{ab}, \qquad (16)$$

one needs to sum the transmission coefficients T_{ab} of waves with unit flux coming in channel a and going out to channel b. In an optical experiment, however, the incoming diffuse beam may have angular weights that differ by a factor of order unity. When using integrating spheres one measures the outgoing intensity, rather than the outgoing flux. As compared to the electronic case, it does not bring a factor μ_b to the weight of the outgoing channel. As these differences between electronic and optical measurements only lead to different numerical prefactors,

we calculate the optical UCF with the same weights as in the electronic case. Summing (9) over the channels a yields a source for the diffuse intensity:

$$S(z) = \sum_a S_a = \frac{2k}{\ell} \int_0^1 d\mu e^{-z/\ell\mu_a}. \tag{17}$$

This is again the input in the Schwarzschild-Milne equation (11). In the bulk the intensity now has the diffusive behavior

$$\mathcal{L}^{\rm in}(z) = \frac{4k}{\ell} \frac{L + z_0 - z}{L + 2z_0}. \tag{18}$$

This object has been termed the incoming *total-flux diffuson* [25]. It has the same depth dependence as $\mathcal{L}^a_{\rm in}$, but contains a different prefactor. Defining

$$\epsilon_a = \frac{\pi T(\mu_a)\tau_1(\mu_a)}{k_1^2 m^2 A \mu_a}, \tag{19}$$

we can verify the sum rule

$$\sum_a \epsilon_a = \int \frac{d^2Q}{(2\pi^2)} \frac{\pi T(\mu)\tau_1(\mu)}{k_1^2 m^2 \mu} = \frac{1}{2} \int d\mu T(\mu)\tau_1(\mu) = 1. \tag{20}$$

Here we used that $k = mk_1$, the definition $\mu = \sqrt{1 - Q^2/k^2}$, and (2.30) of Ref. [26]. One thus has

$$\mathcal{L}^a_{\rm in}(z) = \epsilon_a \mathcal{L}_{\rm in}(z). \tag{21}$$

On the outgoing side, radiation emitted at a point $r = (\rho, z)$ inside the slab will propagate to a point (Z, ρ') outside the sample ($Z > L$) as described by the Green's function of a semi-infinite medium with dielectric function $\epsilon(\mathbf{r}) = \epsilon_0$ for $z < L$ and $\epsilon(\mathbf{r}) = \epsilon_1$ for $z > L$,

$$G(\rho, z; \rho', Z) = \frac{1}{A} \sum_Q G(z; Z; Q) e^{iQ(\rho - \rho')}, \tag{22}$$

in which $G(z; Z; Q)$ is the one-dimensional (1D) Fourier transform of Eq. (5),

$$G(z; Z; Q) = \frac{i}{P + p} e^{iP(L-z) + ip(Z-L)},$$
$$P = \sqrt{k^2 - Q^2 + nt}, \qquad p = \sqrt{k_1^2 - Q^2}. \tag{23}$$

In the far field ($Z \gg L$) the total transmitted intensity reads

$$\int d^2\rho' |G(\rho, z; \rho', Z)|^2 = \frac{1}{A} \sum_Q |G(z; Z; Q)|^2. \tag{24}$$

Since $p_z = k_1 \cos\theta_a = k\mu_a$, the corresponding flux is

$$\Phi(z) = \frac{1}{A} \sum_Q k\mu |G(z; Z; Q)|^2 = \frac{k}{8\pi} \int_0^1 d\mu e^{-(L-z)/\ell\mu}. \tag{25}$$

It leads to a source $S(z) = 4\pi\Phi(z)/\ell$ in the Schwarzschild-Milne equation. The outgoing total-flux diffuson in transmission therefore reads

$$\mathcal{L}_{\rm out}(z) = \frac{k}{\ell} \frac{z + z_0}{L + 2z_0}. \tag{26}$$

Apart from a reflection, this expression differs by a factor of 4 from (18). The prefactors would be the same if our Green's functions were multiplied by a factor of 2; this amounts to the same as taking a kinetic term $\nabla^2/2$ rather than ∇^2, such as occurs in electronics in units where $\hbar = m = 1$.

For the outgoing intensity in the direction b one has, in analogy with (21),

$$\mathcal{L}^b_{\rm out}(z) = \epsilon_b \mathcal{L}_{\rm out}(z). \tag{27}$$

We call the incoming and outgoing diffusons *external* diffusons, because they are connected to the outside of the sample. This is in contrast to the *internal* diffusons that begin and end at interference vertices inside the medium. Away from the surface the internal diffusons obey the well known diffusion equation $\nabla^2 \mathcal{L}_{\rm int}(r) = 12\pi\delta(r - r')/\ell^3$.

The result for the angle resolved transmission of Nieuwenhuizen and Luck [26] can be written as

$$\langle T \rangle_{ab} = \epsilon_a \epsilon_b \langle T \rangle, \tag{28}$$

where $\langle T \rangle$ is the average conductance

$$\langle T \rangle = \frac{k^2 A \ell}{3\pi(L + 2z_0)} \tag{29}$$

in dimensionless units. Restoring units for the electronic case one has for the average conductance

$$\langle G \rangle = \frac{2e^2}{h} \frac{k^2 A \ell}{3\pi(L + 2z_0)}. \tag{30}$$

All the above can be generalized to include absorbing scatterers and frequency differences between incoming beams. For an electronic system the corresponding effects would be a change in Fermi energy, rather than a change in frequency, and the effect of a finite incoherence length, rather than the effect of absorption. For this more general case the diffusion equation reads

$$[-\nabla^2 + \kappa^2 + i\Omega]\mathcal{L}_{\rm int}(r) = \frac{12\pi}{\ell^3} \delta(r - r'). \tag{31}$$

The inverse absorption length κ is related to the albedo a as $\kappa^2 = 3(1 - a)/\ell^2$; $\Omega = \Delta\omega/D$ is the ratio of the frequency difference of the amplitude propagators and the diffusion constant D. It holds that $D = \frac{1}{3} v_E \ell$, where v_E is the transport speed [30]. In the slab geometry after Fourier transform in the z direction the diffusons obey

$$-\frac{d^2}{dz^2} \mathcal{L}_{\rm int}(z, z'; M) + M^2 \mathcal{L}_{\rm int}(z, z'; M) = \frac{12\pi}{\ell^3} \delta(z - z'), \tag{32}$$

where we have defined the decay rate

$$M^2 = Q^2 + \kappa^2 + i\Omega. \tag{33}$$

The complex parameter M describes the exponential decay $\mathcal{L} \sim \exp(-Mz)$ of the diffuse intensity in the z direction. The solutions to the diffusion equation are a linear combination of hyperbolic sines and cosines. In conductance measurements using integrating spheres, external diffusons with momentum or frequency terms yield no contribution, and thus $M = \kappa$ for the external diffusons, i.e.,

$$\mathcal{L}_{\rm in}(z) = \frac{4k}{\ell} \frac{\sinh[\kappa(L-z)] + \kappa z_0 \cosh[\kappa(L-z)]}{(1+\kappa^2 z_0^2)\sinh \kappa L + 2\kappa z_0 \cosh \kappa L}, \quad (34a)$$

$$\mathcal{L}_{\rm out}(z) = \frac{k}{\ell} \frac{\sinh \kappa z + \kappa z_0 \cosh \kappa z}{(1+\kappa^2 z_0^2)\sinh \kappa L + 2\kappa z_0 \cosh \kappa L}, \quad (34b)$$

whereas for the internal diffusons

$$\mathcal{L}_{\rm int}(z,z';M) = \frac{12\pi}{\ell^3} \frac{\{\sinh Mz + Mz_0 \cosh Mz\}\{\sinh[M(L-z')] + Mz_0 \cosh[M(L-z')]\}}{(M+M^3 z_0^2)\sinh ML + 2M^2 z_0 \cosh ML}, \quad (35)$$

where it is assumed that $z < z'$, otherwise z and z' must be interchanged on the right-hand side (RHS). With equal indices of refraction inside and outside the sample the extrapolation length z_0 is, as stated above, 0.7104ℓ and thus the terms involving z_0 yield contributions of the order ℓ/L. For optically thick samples ($L \gg \ell$) one has

$$\mathcal{L}_{\rm int}(z,z';M) = \frac{12\pi}{\ell^3} \frac{\sinh Mz \sinh[M(L-z')]}{M \sinh ML}. \quad (36)$$

Consistent with this expression the boundary conditions become approximately $\mathcal{L}_{\rm int}(0,z') = \mathcal{L}_{\rm int}(L,z') = 0$. If there is an index mismatch, the surfaces partially reflect and the extrapolation length z_0 increases [26]. Internal reflection becomes especially important when z_0 becomes comparable to the sample thickness. Such may occur for large index mismatch and moderate thicknesses.

The C_3 correlation function, defined in (1), involves incoming diffusons $\mathcal{L}_{\rm in}^{a,c}$ and outgoing ones $\mathcal{L}_{\rm out}^{b,d}$. Due to the factorization of external direction dependence [see (21), (27), and (29)], it cancels from C_3. We can write

$$C_3^{abcd}(\kappa,\Omega) = C_3(\kappa,\Omega) = \frac{1}{\langle T\rangle^2} \sum_Q F(Q,\kappa,\Omega), \quad (37)$$

where Q is the two-dimensional transversal momentum. The function F is the main object to be determined in this paper. It is thus calculated at fixed Q and with external diffusons being total-flux diffusons. One finds from (1) and (37) the conductance fluctuations

$$\begin{aligned} C_T(\kappa,\Omega) &= \langle T(\omega)T(\omega+\Delta\omega)\rangle - \langle T(\omega)\rangle\langle T(\omega+\Delta\omega)\rangle \\ &= \sum_{abcd} \langle T\rangle_{ab}\langle T\rangle_{cd} C_3 \\ &= \sum_Q F(Q,\kappa,\Omega) \\ &= \begin{cases} F(0,\kappa,\Omega), & \text{quasi 1D} \quad (38a) \\ W\int \frac{dQ}{2\pi} F(Q,\kappa,\Omega), & \text{quasi 2D} \quad (38b) \\ W^2 \int \frac{d^2Q}{(2\pi)^2} F(Q,\kappa,\Omega) & \text{3D.} \quad (38c) \end{cases} \end{aligned}$$

For electronic systems one finds

$$\langle G(k)G(k+\tfrac{1}{3}\ell\Omega)\rangle - \langle G(k)\rangle\langle G(k+\tfrac{1}{3}\ell\Omega)\rangle = \left(\frac{2e^2}{h}\right)^2 C_T(0,\Omega). \quad (39)$$

These results can be extended for other geometries. If the width is comparable to the thickness of the slab, the momentum integral discretizes into a sum over transversal eigenmodes [4]. The result can be generalized further to arbitrary geometries by taking x,y dependence into account, and calculating the diffusons using appropriate boundary conditions.

III. LONG RANGE DIAGRAMS

At this point we address the structure of the leading diagrams for the correlation functions, defined in (1). For all diagrams there are two incoming advanced fields, which we momentarily term i and j, and two retarded ones, i^* and j^*. The first term on the RHS in Eq. (1) follows from the diagram where i and i^* are paired into an incoming diffuson, and the same for j and j^*. These diffusons have no common scatterers, so for this contribution the expression factorizes into a product of averages. For the C_1 term in (1) such a factorization also takes place [12]. However, in this term the pairings are ij^* and ji^*. In the C_2 correlation function there are two terms. In the first the incoming diffusons have pairings ij^* and ji^*. These diffusons interfere in some point in space, where they exchange partners. The outgoing pairings are then ii^*, jj^*. It is this term that contributes in measurements of the total transmission. The time-inversed diagram, with the in- and outgoing part of the diagram interchanged, also contributes to Eq. (1). However, it does not contribute when this expression is summed over b and d, i.e., in total transmission.

Interference of diffusons occurs if they exchange an amplitude in the presence of a common scatterer. In diagrammatic language this is described by so called Hikami vertices [31,32]. They are in Fig. 2 depicted as shaded polygons; the four-point vertex represents the interference of four diffusons, and the six-point vertex connects six diffusons. The shaded polygons in the figure indicate that the vertices are dressed; in second order Born approximation the dressed four-point vertex is the sum of three diagrams, and the six-point vertex is the sum of sixteen diagrams [32].

In electronic experiments where one measures the conductivity, and in optical experiments where one uses an integrating sphere on the incoming side for creating a diffuse beam, the two amplitudes in the diffuson must have

exactly the same phase. Therefore the incoming diffusons cannot have a momentum or frequency difference, and the pairing must be ii^* and jj^*. In Fig. 2(a) the incoming diffusons interfere somewhere in the slab. In diagrammatic language the diffusons interchange a propagator so that the pairing is changed into ij^* and ji^*. Propagation continues with these diffusons, which, due to the different pairing, can have nonzero frequency difference and nonzero momentum. But in order to be dominant the outgoing diffusons can also not have a momentum or frequency difference. Therefore somewhere else in the slab a second interference occurs. Again exchanging an amplitude, the original pairing, ii^* and jj^*, is restored and the two diffusons propagate out; see Fig. 2(a)i. Some other contributions occur as well. Whereas the incoming and outgoing pairings are always ii^* and jj^*, the internal ones may be different. In Fig. 2(a)ii the first incoming diffuson meets an outgoing diffuson and amplitudes are exchanged. These internal diffusion lines meet at a second point where the original pairings are restored. It is clear that in this process the intermediate paths are traversed in time-reversed order. Due to time-reversal symmetry they give a similar contribution to the previous Fig. 2(a)i. In Fig. 2(b)i, for instance, a diffuson breaks up such that one of its amplitudes makes a large detour, returns to the breaking point, and recombines into an outgoing diffuson. The second incoming diffuson crosses this excess path of the amplitude, and one of its amplitudes follows exactly the same contour as the one of the first diffuson. The fourth amplitude resides and finally recombines with its original partner amplitude to form an outgoing diffuson. Finally, Fig. 2(c) depicts the situation where only one internal diffuson occurs. Its end points must lie within a distance of a few mean free paths. Because of its local character this class does not show up in the final result; it is needed, however, in the regularization process, since it contains terms that cancel divergencies from the other two classes.

Due to the diffusive behavior of the internal propagators we call all these the "long range diagrams." Their internal lines are diffusons (ladder diagrams), that is to say, in these lines there can be an arbitrary number of scatterers. Note that these long range diagrams also include terms with only a small number of scatterers, e.g., one or two. The latter contributions are, of course, not really long range; however, they contribute to the geometric series that represents the ladder diagram. We state this explicitly, since below we will discuss some unexpected problems of these short ranged contributions to the long range diagrams. There are also some special short ranged contributions. Due to various subtleties, they resist a general treatment; their calculation is postponed to Sec. VI.

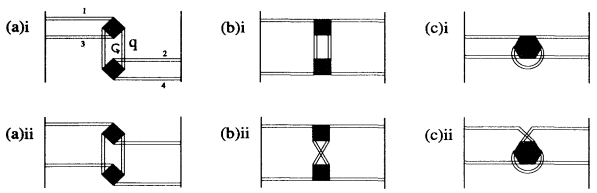

FIG. 2. The leading contributions to the conductance fluctuations, apart from some special short distance processes dealt with in Sec. VI. The incoming diffusons from the left interfere twice before they go out on the right. The close parallel lines correspond to diffusons; the shaded boxes are Hikami vertices; $\mathbf{q}$ denotes the free momentum which is to be integrated over.

Another class of diagrams can be constructed by taking the upper half of Fig. 2(a)ii and combining it with the lower half of Fig. 2(b)i. This diagram contains again two four-point vertices and also two internal diffusons. It is easily seen that incoming amplitudes ii^* and jj^* are mixed into ij^* and ji^*. These new diagrams are $1/g^2$ corrections to the angular dependent C_2 and as such do not contribute in conductance measurements.

IV. DIVERGENCIES IN THE DIFFUSION APPROXIMATION

The diagrams for the conductance fluctuations contain a loop; the two internal diffusons have a free momentum, over which one has to integrate. In Fig. 2(a) this momentum is denoted $\mathbf{q}$. Physically, one expects important contributions to the conductance fluctuations if the distance between the two interference vertices ranges from the mean free path to the sample size. But in this section we will show that the $\mathbf{q}$ integral for the long range diagrams diverges for large momentum, i.e., when the two interference processes are close to each other. The standard picture of diffuse transport with diffusons and interference described by Hikami vertices, which works so well for loopless diagrams such as the C_2 correlation function [15] and the third cumulant of the total transmission [33], now becomes spoiled by these divergencies. In Sec. VI we solve the problem by going back to mesoscopic scales and considering all scattering events.

The problem becomes clear if we calculate the diagrams of Fig. 2. First, we need the expressions for the Hikami vertices. In order to derive the vertices, the momenta are expanded to leading order in $(\mathbf{q}\ell)$. For large $\mathbf{q}\ell$ this is in principle not allowed, but in practice it could still work. The four-point vertex and the six-point vertex are found by summation of the bare vertex and its dressings. The calculation has been reported several times in the literature [11,29,32]. We include the effects of absorption and frequency differences and find

$$H_4 = h_4\left[-\mathbf{q}_1\cdot\mathbf{q}_3 - \mathbf{q}_2\cdot\mathbf{q}_4 + \frac{1}{2}\sum_{i=1}^{4}(\mathbf{q}_i^2 + \kappa_i^2 + i\Omega_i)\right], \tag{40a}$$

$$H_6 = -h_6\left[\mathbf{q}_1\cdot\mathbf{q}_2 + \mathbf{q}_2\cdot\mathbf{q}_3 + \mathbf{q}_3\cdot\mathbf{q}_4 + \mathbf{q}_4\cdot\mathbf{q}_5 + \mathbf{q}_5\cdot\mathbf{q}_6 + \mathbf{q}_6\cdot\mathbf{q}_1 + \sum_{i=1}^{6}\left(\mathbf{q}_i^2 + \frac{1}{2}\kappa_i^2 + \frac{i}{2}\Omega_i\right)\right]. \tag{40b}$$

We call these the "invariant" forms of H_4 and H_6 as they are unchanged under the shifts $\mathbf{q}_i \to \mathbf{q}_i - \frac{1}{4}\sum_{j=1}^{4}\mathbf{q}_j$, $\mathbf{q}_i \to \mathbf{q}_i - \frac{1}{6}\sum_{j=1}^{6}\mathbf{q}_j$, respectively. We defined the prefactors as

$$h_4 = \frac{\ell^5}{48\pi k^2}, \qquad h_6 = \frac{\ell^7}{96\pi k^4}. \tag{41}$$

The momenta of the diffusons that are attached to these vertices are denoted by $\mathbf{q}_i$, where the diffusons are numbered clockwise on the vertex and their momenta are directed towards the vertex. In the actual calculations the Fourier transforms in the z direction of the vertices are used. Compared to previous results of, for instance, Hikami [32], the vertices contain additional frequency and absorption terms. According to the diffusion equation (32) these extra terms together with the $\mathbf{q}^2$ terms lead to a source $\delta(z-z')$. For external diffusons, such terms are neglected as they bring contributions of the order ℓ/L. This approximation simplified the calculation of, for instance, the long range correlation function [15]. For the internal diffusons, however, the source terms are of leading order and cause divergencies. They correspond to the situation where the two interferences take place within a distance of a few mean free paths.

As an example we calculate the diagram presented in Fig. 2(a)i. This diagram was first depicted by Feng, Kane, Lee, and Stone [12] and considered in detail by Berkovits and Feng [11]. These authors pointed out that a short distance divergency appears. For the case of external momenta approximately zero, the Hikami box (40) yields $H_4(\mathbf{q},0,-\mathbf{q},0) = 2h_4q^2$, while the internal diffuson has the form $\mathcal{L}_{\rm int}(q) = 12\pi/(\ell^3q^2)$. Omitting the external lines the diagram Fig. 2(a)i then simply leads to

$$\int \frac{d^3q}{(2\pi)^3} H_4^2(\mathbf{q},0,-\mathbf{q},0)\mathcal{L}_{\rm int}^2(q) = \frac{\ell^4}{4k^4}\int\frac{d^3q}{(2\pi)^3}q^0 = \frac{\ell^4}{4k^4}\delta^{(3)}(\mathbf{r}=\mathbf{0}), \tag{42}$$

which is indeed a cubic divergency in three dimensions, and, more generally, a d-dimensional divergency in d dimensions. As it is arising from the physically innocent situation where the two interference vertices are close to each other, we expect that the divergency has to disappear finally.

We now calculate the diagram for the slab geometry. For simplicity we first consider a quasi-one-dimensional system in which frequency differences and absorption are absent and therefore the decay rate ("mass") vanishes, i.e., $M = 0$ for all diffusons. (Beyond quasi 1D one would have to take nonzero $M = Q$ and sum over the allowed Q.) From Fig. 2(a)i one directly read off its corresponding expression $F_{a.i}$

$$F_{a.i} = \int\int dz dz' \mathcal{L}_{\rm in}^2(z)H_4(z)\mathcal{L}_{\rm int}^2(z,z')H_4(z')\mathcal{L}_{\rm out}^2(z). \tag{43}$$

We label the two incoming diffusons 1 and 3, the outgoing ones 2 and 4, and the internal ones $\mathcal{L}(z_5,z_7)$ and $\mathcal{L}(z_6,z_8)$ (with $5,7$ at z and $6,8$ at z'). The real space expressions for the Hikami boxes become

$$H_4(z) = h_4[\partial_{z_1}\partial_{z_3} + \tfrac{1}{2}(\partial_{z_5}+\partial_{z_7})^2 - \partial_{z_5}^2 - \partial_{z_7}^2], \tag{44a}$$

$$H_4(z') = h_4[\partial_{z_2}\partial_{z_4} + \tfrac{1}{2}(\partial_{z_6}+\partial_{z_8})^2 - \partial_{z_6}^2 - \partial_{z_8}^2], \tag{44b}$$

in which ∂_{z_i} is the derivative of the corresponding diffuson; after performing the differentiation $z_{1,3,5,7}$ should be put equal to z, while $z_{2,4,6,8}$ should be put equal to z'. Keeping $z_{2,4,6,8}$ fixed, we obtain for the z integral after some partial integrations

$$\begin{aligned}
&\int_0^L dz H_4(z)\mathcal{L}_{\rm in}(z_1)\mathcal{L}_{\rm in}(z_3)\mathcal{L}_{\rm int}(z_5,z_6)\mathcal{L}_{\rm int}(z_7,z_8)\\
&\quad= \frac{12\pi h_4}{\ell^3}\int dz[\mathcal{L}_{\rm int}(z,z_6)\delta(z-z_8)+\mathcal{L}_{\rm int}(z,z_8)\delta(z-z_6)]\mathcal{L}_{\rm in}^2(z) + 2h_4\int dz\mathcal{L}_{\rm int}(z,z_6)\mathcal{L}_{\rm int}(z,z_8)\mathcal{L}_{\rm in}'^2(z)\\
&\quad= \frac{12\pi h_4}{\ell^3}\mathcal{L}_{\rm int}(z_8,z_6)\mathcal{L}_{\rm in}^2(z_8) + \frac{12\pi h_4}{\ell^3}\mathcal{L}_{\rm int}(z_6,z_8)\mathcal{L}_{\rm in}^2(z_6) + 2h_4\int dz\mathcal{L}_{\rm int}(z,z_6)\mathcal{L}_{\rm int}(z,z_8)\mathcal{L}_{\rm in}'^2(z).
\end{aligned}$$

Here we also used the diffuson equation, which in this simplified case reads $\partial_z^2\mathcal{L}_{\rm in} = 0$ and $\partial_z^2\mathcal{L}_{\rm int}(z,z') = 12\pi\delta(z-z')/\ell^3$. Also, carrying out the z' integral we find after performing again some partial integrations

$$\begin{aligned}
F_{a.i} &= \int dz' H_4(z')\mathcal{L}_{\rm out}(z_2)\mathcal{L}_{\rm out}(z_4)\left[\frac{12\pi h_4}{\ell^3}\mathcal{L}_{\rm int}(z_8,z_6)\mathcal{L}_{\rm in}^2(z_8)\right.\\
&\quad\left.+\frac{12\pi h_4}{\ell^3}\mathcal{L}_{\rm int}(z_6,z_8)\mathcal{L}_{\rm in}^2(z_6) + 2h_4\int dz\mathcal{L}_{\rm int}(z,z_6)\mathcal{L}_{\rm int}(z,z_8)\mathcal{L}_{\rm in}'(z)\right]\\
&= \frac{\ell^4}{4k^4}\delta(0)\int dz\mathcal{L}_{\rm in}^2(z)\mathcal{L}_{\rm out}^2(z)\\
&\quad+\frac{h_4\ell^2}{k^2}\int dz\mathcal{L}_{\rm int}(z,z)[\mathcal{L}_{\rm in}'^2(z)\mathcal{L}_{\rm out}^2(z)+\mathcal{L}_{\rm in}^2(z)\mathcal{L}_{\rm out}'^2(z)+2\mathcal{L}_{\rm in}'(z)\mathcal{L}_{\rm out}'(z)\mathcal{L}_{\rm in}(z)\mathcal{L}_{\rm out}(z)]\\
&\quad+4h_4^2\int dz'\int dz\mathcal{L}_{\rm int}^2(z,z')\mathcal{L}_{\rm in}'^2(z)\mathcal{L}_{\rm out}'^2(z').
\end{aligned} \tag{45}$$

The spatial derivative of $\mathcal{L}(z)$ is denoted $\mathcal{L}'$. All diffusons are simple linear functions in this case, yielding

$$F_{a.i} = \frac{2}{15}\delta(0)L + \frac{8}{45}. \tag{46}$$

Note that the prefactors of the diffusons and the Hikami boxes have canceled precisely. This is closely related to the universal character of conductance fluctuations in electronic systems; see (39).

The term $\delta(0)$ is a linear divergency, which is the cause of all trouble. In the three-dimensional case one has to take $Q \neq 0$. The $\delta(0)L$ term will occur also for transversal momentum $Q \neq 0$, so that the Q sum yields the cubic divergency

$$W^2 \int \frac{d^2Q}{(2\pi)^2}\delta(0)L = W^2 L\delta^{(3)}(0), \tag{47}$$

as expected from the above bulk consideration.

We now give the results of all diagrams of Fig. 2. We no longer restrict ourselves to the $M = 0$ case. The expressions are labeled according to the diagrams in the figure, F_a, F_b, and F_c. In the diagrams of Fig. 2(a), the decay rates of Eq. (33) for the internal diffusons are each other's complex conjugates, M and M^*. In the diagrams of Fig. 2(b) both internal diffusons have the same decay rate. Using the definition of the Hikami vertices and the diffusion equation, we obtain

$$F_a(M) = \frac{\ell^4}{2k^4}\delta(0)\int dz\,\mathcal{L}_{\rm in}^2\mathcal{L}_{\rm out}^2 + \frac{h_4\ell^2}{2k^2}\mathrm{Re}\int dz\,\mathcal{L}_{\rm int}(z,z;M)\left[3\mathcal{L}_{\rm in}'^2\mathcal{L}_{\rm out}^2 + 3\mathcal{L}_{\rm in}^2\mathcal{L}_{\rm out}'^2 + 10\mathcal{L}_{\rm in}'\mathcal{L}_{\rm out}'\mathcal{L}_{\rm in}\mathcal{L}_{\rm out} - 4i\Omega\mathcal{L}_{\rm in}^2\mathcal{L}_{\rm out}^2\right]$$
$$+4h_4^2\int\int dz\,dz'\,\mathcal{L}_{\rm int}(z,z';M)\mathcal{L}_{\rm int}(z,z';M^*)\left[\mathcal{L}_{\rm in}'^2(z)\mathcal{L}_{\rm out}'^2(z') + \mathcal{L}_{\rm in}'(z)\mathcal{L}_{\rm out}'(z)\mathcal{L}_{\rm in}'(z')\mathcal{L}_{\rm out}'(z')\right], \tag{48a}$$

$$F_b(M) = \frac{\ell^4}{4k^4}\delta(0)\int dz\mathcal{L}_{\rm in}^2\mathcal{L}_{\rm out}^2 + \frac{h_4\ell^2}{2k^2}\mathrm{Re}\int dz\,\mathcal{L}_{\rm int}(z,z;M)\left[-2\mathcal{L}_{\rm in}'\mathcal{L}_{\rm out}'\mathcal{L}_{\rm in}\mathcal{L}_{\rm out} + \mathcal{L}_{\rm in}'^2\mathcal{L}_{\rm out}^2 + \mathcal{L}_{\rm in}^2\mathcal{L}_{\rm out}'^2 - 4\kappa^2\mathcal{L}_{\rm in}^2\mathcal{L}_{\rm out}^2\right]$$
$$+\frac{1}{2}h_4^2\int\int dz\,dz'\,\left[\mathcal{L}_{\rm int}^2(z,z';M) + \mathcal{L}_{\rm int}^2(z,z';M^*)\right]\frac{d^2}{dz^2}\left[\mathcal{L}_{\rm in}(z)\mathcal{L}_{\rm out}(z)\right]\frac{d^2}{dz'^2}\left[\mathcal{L}_{\rm in}(z')\mathcal{L}_{\rm out}(z')\right], \tag{48b}$$

$$F_c(M) = -\frac{\ell^4}{k^4}\delta(0)\int dz\,\mathcal{L}_{\rm in}^2\mathcal{L}_{\rm out}^2 - \frac{2h_4\ell^2}{k^2}\mathrm{Re}\int dz\,\mathcal{L}_{\rm int}(z,z;M)$$
$$\times\left[2\mathcal{L}_{\rm in}'\mathcal{L}_{\rm out}'\mathcal{L}_{\rm in}\mathcal{L}_{\rm out} + \mathcal{L}_{\rm in}'^2\mathcal{L}_{\rm out}^2 + \mathcal{L}_{\rm in}^2\mathcal{L}_{\rm out}'^2 - (\kappa^2 + i\Omega)\mathcal{L}_{\rm in}^2\mathcal{L}_{\rm out}^2\right], \tag{48c}$$

where we used the shorthand notation that in the single integrals all incoming and outgoing diffusons have argument z. To obtain the variance of the fluctuations in quasi-one-dimension, F is evaluated at transverse momentum $Q = 0$. The internal momentum Q enters the equations via the decay rate of the internal diffusons, defined by $M^2 = Q^2 + \kappa^2 + i\Omega$. In two and three dimensions a sum or integral over the transversal momentum has to be performed.

In (48a) and (48b) we can distinguish three contributions to F. In the first term, both Hikami boxes operate on the internal diffusons, yielding in the diffusion approximation a δ function evaluated in zero. The resulting term is independent of all the momenta of the external diffusons. It can be seen from the diffusion equation that a diffuson decays rapidly if its momentum becomes large. Terms of the diffusons with few scatterers are dominant at large momentum; they cause the divergence. Our present description of these processes is incomplete. In order to see the cancellation of this divergency, calculation of the long range diagrams is not sufficient, so that the short distance processes have to be examined in detail. This will be done in the next section. The second term of (48a) and (48b) is a single integral; it comes about when the boxes act on one internal and one external diffuson. This corresponds to the case where one internal diffuson is almost empty, while the other diffuson contains an arbitrary number of scatterers. In two and three dimensions the momentum integral diverges, since for large Q it behaves as $\int dz \int d^{d-1}Q\mathcal{L}_{\rm int}(Q;z,z) \sim \int d^{d-1}Q\,Q^{-1}$. But when summing the a, b, and c contribution this term cancels. The sum gives

$$F_a(M) + F_b(M) + F_c(M)$$
$$= -\frac{\ell^4}{4k^4}\delta(0)\int dz\mathcal{L}_{\rm in}^2\mathcal{L}_{\rm out}^2$$
$$+4h_4^2\int\int dz\,dz'\,\mathcal{L}_{\rm int}(z,z';M)\mathcal{L}_{\rm int}(z,z';M^*)\left[\mathcal{L}_{\rm in}'^2(z)\mathcal{L}_{\rm out}'^2(z') + \mathcal{L}_{\rm in}'(z)\mathcal{L}_{\rm out}'(z)\mathcal{L}_{\rm in}'(z')\mathcal{L}_{\rm out}'(z')\right]$$
$$+\frac{1}{2}h_4^2\int\int dz\,dz'\,\left[\mathcal{L}_{\rm int}^2(z,z';M) + \mathcal{L}_{\rm int}^2(z,z';M^*)\right]\frac{d^2}{dz^2}\left[\mathcal{L}_{\rm in}(z)\mathcal{L}_{\rm out}(z)\right]\frac{d^2}{dz'^2}\left[\mathcal{L}_{\rm in}(z')\mathcal{L}_{\rm out}(z')\right]. \tag{49}$$

The last two terms involve a double integral describing interference vertices at different points in space; technically it arises when both boxes act on external diffusons, or from terms where they do so after partial integrations. This term is absent in the expression F_c, which contains only one z dependence as can be seen from Fig. 2(c). When performing the integral of F over the transverse momentum Q, the double integral term behaves at large Q as $\int dz \int dz' \int d^{d-1}Q \mathcal{L}^2_{\rm int}(Q;z,z') \sim \int d^{d-1}Q\, Q^{-3}$. It is thus convergent. One expects that finally only this term will survive. It is also the only contribution depending solely on derivatives of the external diffusons.

In the quasi-one-dimensional case where absorption and frequency terms are absent, the expressions reduce to

$$F_a(0) + F_b(0) + F_c(0) = -\frac{2}{15}\delta(0)L + \frac{2}{15}. \qquad (50)$$

The second part is a well known result for the UCF in one dimension, but a singular part is annoyingly present. Before we can obtain the UCF and correlation functions, we have to show its cancellation. We expect the unphysical divergency to disappear by summing all diagrams and in the next section we set out to find *all* leading diagrams.

V. GENERATING DIAGRAMS THROUGH A GENERALIZED KADANOFF-BAYM TECHNIQUE

Finding the correct and complete set of diagrams by educated guess proves very difficult, especially for the low order diagrams. In this section we pursue the technique founded by Baym and Kadanoff [34,35] to generate all diagrams. This method provides a systematic way to construct the diagrams in a particular approximation. The approximation is made on the level of a generating functional. The form of this functional is guided by intuition or by prior knowledge of the self-energy or some other physical quantity. The theory of Kadanoff and Baym, of which the basics will be reviewed in the course of this section, prescribes which diagrams are to be included in the perturbation theory on *any* level in the hierarchy of the many particle Green's functions. It was proven by Baym and Kadanoff [34,35] that this procedure provides a conserving theory in the sense that sum rules based on conservation of particle number, momentum, angular momentum, or energy are fulfilled. However, it does not guarantee that a sensible theory in a physical or even in a mathematical sense will be produced. (The Green's functions themselves may not possess the correct analytical structure, i.e., they may be non-Herglotz [36].)

The theory of Kadanoff and Baym is defined for interacting electron systems. It is our goal to describe the scattering of light in a disordered medium. The connection between electronic and optical disordered media can be put on a solid footing as the equations which describe these phenomena can be mapped onto each other [6]. The equivalence of interacting and disordered systems, however, is less obvious. Although one can rewrite models of disorder in such a way that an effective interaction is present [37], the precise form of that interaction depends on the physical quantities that are studied. Furthermore, if one wants to represent the disorder as a two-body, central potential, one is limited to special disorder distributions (e.g., Gaussian) or approximations (e.g., second order Born). However, these drawbacks do not hinder us in using this theory in a heuristic sense.

The input of the theory is an approximate functional Φ from which we may derive the perturbation theory. In the choice we are led by the theory of weak localization and universal conductance fluctuations (UCF). The maximally crossed diagrams, which are the most important quantum corrections, are generated by the functional depicted in Fig. 3(a). These wheel-like diagrams are generalized Fock diagrams in the sense that the first term in the sum produces the Fock diagram for the self-energy. The UCF diagrams are generated by a functional which may be called "generalized Hartree" in the same sense; see Figs. 3(b) and 3(c). It turns out that the weak localization effect and the UCF are connected and may be generated from a single diagram [38]. This observation leads to the conjecture that the most important contributions in the intensity fluctuations stem from the same diagrams. We thus adopt the functionals as given in Figs. 3(b) and 3(c) as the ones we start our calculation with.

Let us briefly review the aspects of the Kadanoff and Baym theory we need. Starting with some functional Φ as described above, the self-energy $\Sigma^{\rm I}_{\rm I}$ and the two-particle irreducible vertex $\Sigma^{12}_{\bar{1}\bar{2}}$ may be found from

$$\Sigma^{\rm I}_{\rm I} = \delta\Phi \,/\, \delta G^{\rm I}_{\bar{1}}, \qquad (51a)$$

$$\Sigma^{12}_{\bar{1}\bar{2}} = \delta^2\Phi \,/\, (\delta G^{\rm I}_{\bar{1}}\, \delta G^{2}_{\bar{2}}), \qquad (51b)$$

where the numbers $1, \bar{1}, 2, \ldots$ denote the collection of variables $(\vec{k}_1,\omega_1),(\vec{k}'_1,\omega'_1),(\vec{k}_2,\omega_2),\ldots$ and $G^{\rm I}_{\bar{1}} = -\langle \mathcal{T}\Psi(1)\Psi^+(\bar{1})\rangle$. At this point we generalize these results to obtain irreducible three- and four-particle vertices:

$$\Sigma^{123}_{\bar{1}\bar{2}\bar{3}} = \delta^3\Phi \,/\, (\delta G^{\rm I}_{\bar{1}}\, \delta G^{2}_{\bar{2}}\, \delta G^{3}_{\bar{3}}), \qquad (52a)$$

$$\Sigma^{1234}_{\bar{1}\bar{2}\bar{3}\bar{4}} = \delta^4\Phi \,/\, (\delta G^{\rm I}_{\bar{1}}\, \delta G^{2}_{\bar{2}}\, \delta G^{3}_{\bar{3}}\, \delta G^{4}_{\bar{4}}). \qquad (52b)$$

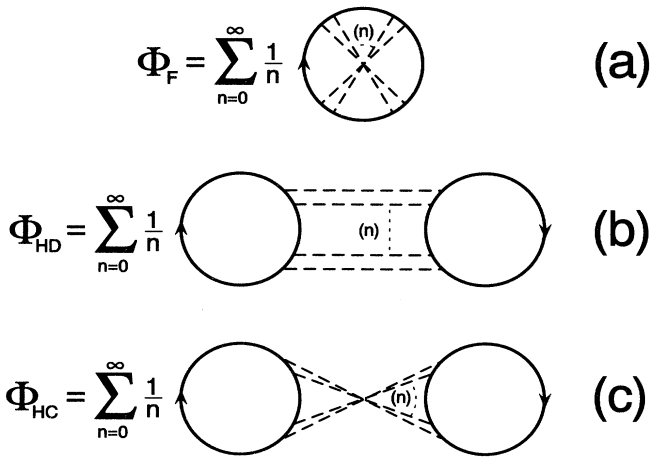

FIG. 3. The generating functional which produces diagrams for (a) weak localization and (b) and (c) the UCF.

Note that these generalizations, like the ones that will follow, are not free from internal symmetry. Since we are primarily interested in the structure of the diagrams, rather than their multiplicativity, we will make no effort to remove this symmetry. The one-particle Green's function $G_1^{\bar{1}}$ is connected to the self-energy by the Dyson equation. A two-particle Green's function $G_{12}^{\bar{1}\bar{2}}$ is connected to the irreducible two-particle vertex by the Bethe-Salpeter equation

$$G_1^{\bar{1}} = G_1^{\bar{1}}(0) + G_1^{\bar{2}}(0)\,\Sigma_{\bar{2}}^{2}\,G_2^{\bar{1}}, \tag{53a}$$

$$G_{12}^{\bar{1}\bar{2}} = G_1^{\bar{2}}\,G_2^{\bar{1}} + G_1^{\bar{3}}\,G_3^{\bar{1}}\,\Sigma_{\bar{3}\bar{4}}^{34}\,G_{42}^{\bar{4}\bar{2}}, \tag{53b}$$

where $G_1^{\bar{1}}(0)$ indicates the bare propagator. Integration over the free variables occurring as super- and subscript is assumed. Again, we may generalize these results to obtain a three-particle Green's function $G_{123}^{\bar{1}\bar{2}\bar{3}}$ and a four-particle Green's function $G_{1234}^{\bar{1}\bar{2}\bar{3}\bar{4}}$. We find [38]

$$G_{123}^{\bar{1}\bar{2}\bar{3}} = (G_5^{\bar{1}}\,G_{13}^{\bar{5}\bar{3}} + G_1^{5}\,G_{53}^{\bar{1}\bar{3}})(\delta_2^{5}\,\delta_5^{\bar{2}} + \Sigma_{\bar{4}\bar{5}}^{45}\,G_{24}^{\bar{2}\bar{4}}) + G_4^{\bar{1}}G_1^{\bar{4}}\,(\Sigma_{\bar{4}\bar{5}}^{45}\,G_{235}^{\bar{2}\bar{3}\bar{5}} + \Sigma_{\bar{4}\bar{5}\bar{6}}^{456}\,G_{36}^{\bar{3}\bar{6}}\,G_{25}^{\bar{2}\bar{5}}), \tag{54a}$$

$$\begin{aligned} G_{1234}^{\bar{1}\bar{2}\bar{3}\bar{4}} &= (G_{534}^{\bar{1}\bar{3}\bar{4}}\,G_1^{5} + G_{53}^{\bar{1}\bar{3}}\,G_{14}^{\bar{5}\bar{4}} + G_{54}^{\bar{1}\bar{4}}\,G_{13}^{\bar{5}\bar{3}} + G_5^{3}\,G_{134}^{\bar{5}\bar{3}\bar{4}})(\delta_2^{5}\,\delta_5^{\bar{2}} + \Sigma_{\bar{5}\bar{6}}^{56}\,G_{26}^{\bar{2}\bar{6}}) \\ &\quad + (G_{58}^{\bar{1}\bar{8}}\,G_1^{5} + G_5^{\bar{1}}\,G_{18}^{\bar{5}\bar{8}})(\Sigma_{\bar{5}\bar{6}\bar{7}}^{567}\,G_{79}^{\bar{7}\bar{9}}\,G_{26}^{\bar{2}\bar{6}} + \Sigma_{\bar{5}\bar{6}}^{56}\,G_{269}^{\bar{2}\bar{6}\bar{9}})(\delta_3^{8}\,\delta_8^{\bar{3}}\,\delta_4^{9}\,\delta_9^{\bar{4}} + \delta_4^{8}\,\delta_8^{\bar{4}}\,\delta_3^{9}\,\delta_9^{\bar{3}}) \\ &\quad + G_5^{\bar{1}}\,G_1^{5}\,(\Sigma_{\bar{5}\bar{6}\bar{7}\bar{8}}^{5678}\,G_{48}^{\bar{4}\bar{8}}\,G_{37}^{\bar{3}\bar{7}}\,G_{26}^{\bar{2}\bar{6}} + \Sigma_{\bar{5}\bar{6}\bar{7}}^{567}\,(G_{347}^{\bar{3}\bar{4}\bar{7}}\,G_{26}^{\bar{2}\bar{6}} + G_{37}^{\bar{3}\bar{7}}\,G_{246}^{\bar{2}\bar{4}\bar{6}} + G_{47}^{\bar{4}\bar{7}}G_{236}^{\bar{2}\bar{3}\bar{6}}) + \Sigma_{\bar{5}\bar{6}}^{56}\,G_{2346}^{\bar{2}\bar{3}\bar{4}\bar{6}})\,, \end{aligned} \tag{54b}$$

where the δ's are Kronecker deltas. These equations provide the full information on the fluctuations in transport quantities given the exact set of irreducible vertices $\Sigma_{\bar{1}}^{1}, \Sigma_{\bar{1}\bar{2}}^{12}, \Sigma_{\bar{1}\bar{2}\bar{3}}^{123}, \Sigma_{\bar{1}\bar{2}\bar{3}\bar{4}}^{1234}$. An approximation of this set can be found by choosing a suitable functional Φ.

The functional we adopt is

$$\Phi := G_1^{\bar{1}}\,G_2^{\bar{2}}\left(-S_{\bar{1}\bar{2}}^{12} + \sum_{n=1}^{\infty} \tfrac{1}{n} L_{\bar{1}\bar{2}}^{12}[n] + \tfrac{1}{n} C_{\bar{1}\bar{2}}^{12}[n]\right), \tag{55}$$

where $L_{\bar{1}\bar{2}}^{12}[n]$ and $C_{\bar{1}\bar{2}}^{12}[n]$ are the product of n scattering terms in the particle-hole and particle-particle channels, respectively. The last two terms are the ones depicted in Figs. 3(b) and 3(c). Algebraically we have

$$S_{\bar{1}\bar{2}}^{12} = L_{\bar{1}\bar{2}}^{12}[1] = C_{\bar{1}\bar{2}}^{12}[1] = \delta_{\bar{2}}^{1}\,\Gamma\,\delta_{\bar{1}}^{2}, \tag{56a}$$

$$L_{\bar{1}\bar{2}}^{12}[n] = S_{\bar{1}\bar{3}}^{13}\,G_4^{\bar{3}}\,G_3^{\bar{4}}\,S_{\bar{4}\cdot}^{4\cdot}\cdots S_{\cdot\bar{2}}^{\cdot 2}, \tag{56b}$$

$$C_{\bar{1}\bar{2}}^{12}[n] = S_{\bar{1}\bar{2}}^{34}\,G_4^{\bar{3}}\,G_3^{\bar{4}}\,S_{\bar{4}\bar{3}}^{\cdot\cdot}\cdots S_{\cdot\cdot}^{44}, \tag{56c}$$

where Γ is the scattering strength in second order Born approximation. After differentiation of Φ with respect to G ladder diagrams and maximally crossed diagrams appear. Each element in these series has prefactor 1. Therefore we define the full ladders in both channels as

$$L_{\bar{1}\bar{2}}^{12} = S_{\bar{1}\bar{2}}^{12} + S_{\bar{1}\bar{3}}^{13}\,G_4^{\bar{3}}\,G_3^{\bar{4}}\,L_{\bar{4}\bar{2}}^{42} = \sum_{n=1}^{\infty} L_{\bar{1}\bar{2}}^{12}[n], \tag{57a}$$

$$C_{\bar{1}\bar{2}}^{12} = S_{\bar{1}\bar{2}}^{12} + S_{\bar{1}\bar{2}}^{43}\,G_4^{\bar{3}}\,G_3^{\bar{4}}\,C_{\bar{4}\bar{3}}^{12} = \sum_{n=1}^{\infty} C_{\bar{1}\bar{2}}^{12}[n]. \tag{57b}$$

Systematic application of Eqs. (51) and (52) on the functional (55) leads to the following irreducible n-particle vertices:

$$\Sigma_{\bar{1}}^{1} = G_2^{\bar{2}}\,(L_{\bar{2}\bar{1}}^{12} + C_{\bar{2}\bar{1}}^{12} - S_{\bar{2}\bar{1}}^{12}), \tag{58a}$$

$$\Sigma_{\bar{1}\bar{2}}^{12} = L_{\bar{2}\bar{1}}^{12} + C_{\bar{2}\bar{1}}^{12} - S_{\bar{2}\bar{1}}^{12} + G_3^{\bar{3}}\,G_4^{\bar{4}}\,(L_{\bar{1}\bar{4}}^{32}\,L_{\bar{3}\bar{2}}^{14} + L_{\bar{1}\bar{2}}^{34}\,L_{\bar{3}\bar{4}}^{12} + C_{\bar{1}\bar{4}}^{32}\,C_{\bar{3}\bar{2}}^{14} + C_{\bar{1}\bar{4}}^{23}\,C_{\bar{2}\bar{3}}^{14}), \tag{58b}$$

$$\begin{aligned} \Sigma_{\bar{1}\bar{2}\bar{3}}^{123} &= \mathrm{Per}_{\bar{1}\bar{2}\bar{3}}^{123}\,\{G_5^{\bar{5}}\,(L_{\bar{1}\bar{2}}^{\bar{3}5}\,L_{\bar{3}5}^{12} + C_{\bar{1}\bar{2}}^{\bar{3}5}\,C_{\bar{3}5}^{12}) \\ &\quad + G_5^{\bar{5}}\,G_6^{\bar{6}}\,G_7^{\bar{7}}\,(\tfrac{1}{3} L_{\bar{5}\bar{2}}^{\bar{1}6}\,L_{\bar{1}3}^{\bar{5}7}\,L_{\bar{3}\bar{6}}^{\bar{7}2} + L_{\bar{5}2}^{\bar{1}6}\,L_{\bar{1}3}^{\bar{5}7}\,L_{\bar{7}\bar{6}}^{\bar{3}2} + \tfrac{1}{3} C_{\bar{5}2}^{\bar{1}6}\,C_{\bar{1}\bar{6}}^{\bar{7}3}\,C_{\bar{3}7}^{\bar{5}2} + C_{\bar{5}2}^{\bar{1}6}\,C_{\bar{1}\bar{6}}^{\bar{3}7}\,C_{\bar{7}3}^{\bar{5}2})\}\,, \end{aligned} \tag{58c}$$

$$\begin{aligned} \Sigma_{\bar{1}\bar{2}\bar{3}\bar{4}}^{1234} &= \mathrm{Per}_{\bar{1}\bar{2}\bar{3}\bar{4}}^{1234}\,\{\tfrac{1}{4}(L_{\bar{1}\bar{2}}^{\bar{3}\bar{4}}\,L_{\bar{3}\bar{4}}^{12} + C_{\bar{1}\bar{2}}^{\bar{3}\bar{4}}\,C_{\bar{3}\bar{4}}^{12}) \\ &\quad + G_5^{\bar{5}}\,G_6^{\bar{6}}\,(L_{\bar{1}\bar{4}}^{\bar{3}5}\,L_{\bar{6}2}^{\bar{4}5}\,L_{\bar{3}5}^{12} + \tfrac{1}{2} L_{\bar{1}\bar{6}}^{\bar{3}4}\,L_{\bar{4}2}^{\bar{6}5}\,L_{\bar{3}5}^{12} + \tfrac{1}{2} L_{\bar{1}2}^{\bar{3}5}\,L_{\bar{3}4}^{\bar{1}6}\,L_{\bar{6}5}^{\bar{4}2} + C_{\bar{1}2}^{\bar{4}6}\,C_{\bar{6}4}^{\bar{3}5}\,C_{\bar{3}5}^{12} + C_{\bar{1}2}^{\bar{6}4}\,C_{\bar{4}6}^{\bar{3}5}\,C_{\bar{3}5}^{12}) \\ &\quad + G_5^{\bar{5}}\,G_6^{\bar{6}}\,G_7^{\bar{7}}\,G_8^{\bar{8}}(\tfrac{1}{6} L_{\bar{1}8}^{\bar{5}4}\,L_{\bar{4}7}^{\bar{8}3}\,L_{\bar{3}6}^{\bar{7}2}\,L_{\bar{5}2}^{\bar{1}6} + L_{\bar{1}4}^{\bar{5}8}\,L_{\bar{8}7}^{\bar{4}3}\,L_{\bar{3}6}^{\bar{7}2}\,L_{\bar{5}2}^{\bar{1}6} + \tfrac{1}{2} L_{\bar{1}4}^{\bar{5}8}\,L_{\bar{8}3}^{\bar{4}7}\,L_{\bar{7}6}^{\bar{3}2}\,L_{\bar{5}2}^{\bar{1}6} + \tfrac{1}{2} L_{\bar{1}3}^{\bar{5}7}\,L_{\bar{7}6}^{\bar{3}2}\,L_{\bar{5}8}^{\bar{1}4}\,L_{\bar{4}2}^{\bar{8}6} \\ &\quad + \tfrac{1}{6} C_{\bar{1}8}^{\bar{8}4}\,C_{\bar{4}8}^{\bar{7}3}\,C_{\bar{3}7}^{\bar{5}2}\,C_{\bar{5}2}^{\bar{1}6} + C_{\bar{1}8}^{\bar{4}8}\,C_{\bar{8}4}^{\bar{7}3}\,C_{\bar{3}7}^{\bar{5}2}\,C_{\bar{5}2}^{\bar{1}6} + \tfrac{1}{2} C_{\bar{1}8}^{\bar{4}8}\,C_{\bar{8}4}^{\bar{3}7}\,C_{\bar{7}3}^{\bar{5}2}\,C_{\bar{5}2}^{\bar{1}6} + \tfrac{1}{4} C_{\bar{1}8}^{\bar{3}7}\,C_{\bar{7}3}^{\bar{5}2}\,C_{\bar{5}2}^{\bar{8}4}\,C_{\bar{4}8}^{\bar{1}6})\}\,, \end{aligned} \tag{58d}$$

where the operator $\mathrm{Per}_{\bar{1}\bar{2}\cdots\bar{n}}^{12\cdots n}$ produces all the permutations of its operand in the variables $(1,\bar{1}),(2,\bar{2}),\ldots,(n,\bar{n})$, i.e., $n!$ diagrams. Expansion of Eq. (54) using Eq. (58) is obviously a considerable task. Taking into account that we only need those diagrams which are different in a topological sense, the effort stays manageable. As usual, diagrams which contain loops do not contribute.

To illustrate the procedure set out above we have a closer look at two examples. First of all, part of the integral equation for $G_{1234}^{\bar{1}\bar{2}\bar{3}\bar{4}}$ is needed. The relevant part is depicted in Fig. 4. Then, in Fig. 5(a) we start off with the functional as depicted in Fig. 3(b). Successive functional differentiation (cutting) as prescribed in Eqs. (51) and (52) produces the one-, two-, three-, and four-particle irreducible vertices given in Figs. 5(b), 5(c), 5(d), and 5(e), respectively. Insertion (gluing) of the latter irreducible four-particle vertex in Fig. 4 amounts to adding external diffusons. Of course, more diagrams are produced in this particular example but for the sake of simplicity no attention is paid to these diagrams.

In the second example we start off with the diagram

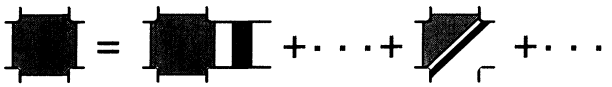

FIG. 4. Part of the integral equation from Eq. (54b). First indicated term on the RHS produces the external ladders.

containing the maximally crossed vertex, Figs. 6(a) or 3(c). By functional differentiation, see Figs. 6(b) and 6(c), and subsequent integration in the Bethe-Salpeter equation (53), we obtain a contribution which consists of two maximally crossed diagrams with a dressing. This element is the input for Eq. (54b), see Fig. 4, and generates an important contribution to the whole set.

The set of diagrams thus generated by the Kadanoff-Baym approach was verified using a computer program. We developed this program to generate all diagrams with six or less scatterers automatically. After generating the set, the program checks it against double counting. Next, momenta are assigned to all propagators such that momentum conservation is obeyed. It then determines whether a particular diagram is of leading order in $(k\ell)^{-1}$; this is the case if all propagators can have a momentum approximately equal to k. The leading diagrams are expressed in terms of the standard integrals defined in Sec. VI. The subsequent analytical calculation and summation of diagrams were done by hand. The program turns out to be especially useful in determining the precise set of leading short distance diagrams, but also the long distance diagrams of Sec. III were reproduced. It should be mentioned that apart from the diagrams from the Kadanoff-Baym approach we also found extra diagrams; in Sec. VI C they are discussed and it is shown that they cancel.

VI. CANCELLATION OF SHORT DISTANCE CONTRIBUTIONS

In this section we show that the strong divergence that occurs if both Hikami boxes act on internal diffusons cancels. Since a diffuson decays rapidly if its momentum becomes large, terms of the diffusons with few scatterers are dominant when the momentum is large, which causes the divergence. The cancellation is thus shown by considering in great detail the short distance processes.

It turned out that complications arise for diagrams

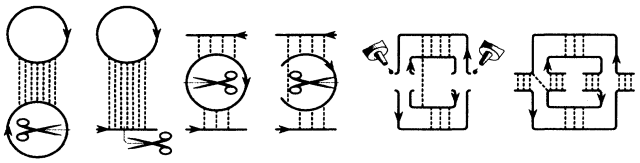

FIG. 5. Particular example of how the double diffuson structure is produced. Functional differention with respect to G is indicated by cutting out a line (pair of scissors) from (a) to (e). Pasting the result in the integral equation, indicated in Fig. 3, results in adding external ladders (glue).

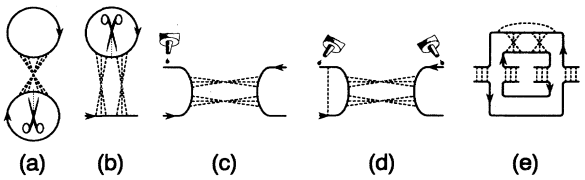

FIG. 6. Particular example of how a set of Cooper propagators is produced. Functional differention with respect to G is indicated by cutting out a line (pair of scissors) from (a) to (e). Pasting the result in the integral equation, indicated in Fig. 3, produces a four-particle quantity (and adds external ladders).

with less than four scatterers. The external diffusons may still contain an arbitrary number of scatterers. For simplicity the calculation in this section is performed in the bulk and the external diffusons are not attached to the diagrams. Since the divergency is independent of the external momenta, the cancellation is generally proven at zero external momentum. For simplicity we may then consider an infinite system. As a result all factors can be expressed in the d-dimensional momentum $\mathbf{q} = (Q, q_z)$. We first look at a fixed value of the d-dimensional internal momentum $\mathbf{q}$ and postpone the integration. We will show that under present conditions the integrand is zero for all $\mathbf{q}$, so that there is no divergency after integration.

All diagrams can be factorized in products of the integrals

$$I^{m,n}_{k,l}(q) = I^{k,l}_{m,n}(q) \equiv \int \frac{d^3\mathbf{p}}{(2\pi)^3} G^k(\mathbf{p}) G^{*l}(\mathbf{p}) G^m(\mathbf{p}+\mathbf{q}) G^{*n}(\mathbf{p}+\mathbf{q}). \tag{59}$$

In the calculation of the diffuson and the Hikami vertices in the previous sections we expanded the integrals in $q\ell$. Since we are after contributions for $q \sim 1/\ell$, this expansion is not allowed. We can still assume that $q \ll k$, as we do not need the physics on length scales comparable to the wavelength, but comparable to one mean free path only. The integrals needed in the calculation are given in Table I, where A_i is an angular average defined as

$$A_i(q) = \frac{1}{4\pi} \int d\hat{\mathbf{p}} \frac{1}{(1+\ell\mathbf{q}\cdot\hat{\mathbf{p}})^i} \qquad (i = 1, 2, 3). \tag{60}$$

The integral for $i = 1$ yields the diffuson kernel $A_1 =$

TABLE I. The short distance diagrams can be factorized in these integrals, defined in Eq. (59); A_i is defined in the text.

$I^{1,0}_{0,1} = \frac{\ell}{4\pi} A_1$	$I^{1,0}_{0,2} = \frac{-i\ell^2}{8\pi k} A_2$
$I^{2,0}_{0,2} = \frac{\ell^3}{8\pi k^2} A_3$	$I^{0,1}_{1,1} = \frac{-i\ell^2}{8\pi k} A_1$
$I^{0,2}_{1,1} = \frac{-\ell^3}{16\pi k^2} A_2$	$I^{1,1}_{1,1} = \frac{\ell^3}{8\pi k^2} A_1$
$I^{0,0}_{1,2} = \frac{-i\ell^2}{8\pi k}$	$I^{0,1}_{1,2} = \frac{-\ell^3}{16\pi k^2} A_1$
$I^{1,0}_{1,2} = \frac{\ell^3}{16\pi k^2}[A_1 + A_2]$	$I^{2,0}_{1,2} = \frac{i\ell^4}{32\pi k^3}[A_2 + 2A_3]$
$I^{1,1}_{1,2} = \frac{-i\ell^4}{32\pi k^3}[2A_1 + A_2]$	$I^{2,1}_{1,2} = \frac{\ell^5}{32\pi k^4}[A_1 + A_2 + A_3]$

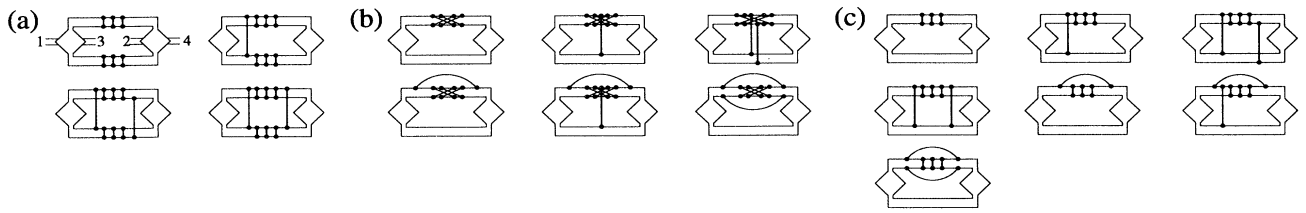

FIG. 7. The dressings of the shaded vertices of Fig. 2 are written out explicitly; this shows the detailed structure of the long range contributions to the conductance fluctuations. The close parallel lines, only explicitly shown in the first diagram, are the external diffusons. Figure 2(a)i corresponds to the case where 1 and 3 are incoming diffusons; Fig. 2(a)ii corresponds to the case where 1 and 2 are incoming diffusons. The vertical, diagonal, or curved lines linking two dots represent a common scatterering of two amplitudes. From top to bottom the horizontal lines in a diagram are advanced, retarded, advanced, and retarded propagators, respectively. The number of scatterers in the internal and external diffusons is arbitrary. Topological equivalent diagrams are not shown. We number the diagrams from left to right and from top to bottom (see Table II).

$\arctan(q\ell)/q\ell$. The internal diffuson now reads

$$\mathcal{L}_{\rm int}(q) = \frac{4\pi}{\ell}\frac{1}{1-A_1}. \tag{61}$$

We recover previous results by expansion in $(q\ell)$. This yields $\mathcal{L}_{\rm int} = 12\pi/(\ell^3 q^2)$ and agrees with the bulk solution of (32).

A. Short distance properties of the long range diagrams

First, look at the long range diagrams with few scatterings. By writing out the dressing of the vertices one obtains the detailed structure of the diagrams, given in Fig. 7. In the diagrams Figs. 2(a)i–2(c)i, the incoming external diffusons are connected to 1 and 3. The diagrams in Figs. 2(a)ii–2(c)ii are obtained by connecting external diffusons 1 and 2 to the incoming side. If such a diagram contains only a few scatterers, it can be grouped into one of the classes of the long range diagrams. A simple example is the upper left diagram of Fig. 7, drawn there with six scatterers. Interchanging the external diffusons numbered 2 and 3 clearly leads to another topology. However, with only two scatterers present, the topology does not change under this operation, and one must be careful not to overcount this term. Bearing this important observation in mind, we sum all long range diagrams for an arbitrary number of scatterers. The expression for each diagram and its combinatorial factor is given in Table II. It is convenient to collect diagrams with an equal number m of scatterers that connect different propagators.

TABLE II. Table used in the calculation of the diagrams presented in Fig. 7 for zero external momenta. The expression for each diagram is given in the second column and its combinatorial prefactor in the other columns for different numbers of scatterers. The last column counts the number of scatterers that are not included as such in the resummmation. There are six diagrams with degeneracy lower than expected: (c)1 for $n = 1$, (a)1,(c)2,(c)5 for $n = 2$, and (c)6,(c)7 for $n = 3$.

Diagram	Expression	$n=1$	$n=2$	$n=3$	$n\geq 4$	$n-m$
(a)1	$\left[I^{1,1}_{1,1}\right]^2\left[I^{1,0}_{0,1}\right]^{n-2}$	0	$1=2-1$	4	$2n-2$	0
(a)2	$I^{1,1}_{1,1}\left[I^{1,0}_{1,1}\right]^2\left[I^{1,0}_{0,1}\right]^{n-3}$	0	0	8	$8n-16$	0
(a)3+(a)4	$\left[I^{0,1}_{1,1}\right]^4\left[I^{1,0}_{0,1}\right]^{n-4}$	0	0	0	$8n-24$	0
(b)1	$I^{0,1}_{2,1}I^{1,0}_{1,2}\left[I^{1,0}_{0,1}\right]^{n-2}$	0	4	8	$4n-4$	0
(b)2	$I^{0,1}_{2,1}\left[I^{1,0}_{1,1}\right]^2\left[I^{1,0}_{0,1}\right]^{n-3}$	0	0	8	$8n-16$	0
(b)3	$\left[I^{0,1}_{1,1}\right]^2\left[I^{1,0}_{1,1}\right]^2\left[I^{1,0}_{0,1}\right]^{n-4}$	0	0	0	$4n-12$	0
(b)4	$I^{0,0}_{2,1}I^{1,0}_{1,2}I^{0,1}_{2,0}\left[I^{1,0}_{0,1}\right]^{n-3}$	0	0	8	$8n-16$	1
(b)5	$I^{0,0}_{2,1}I^{0,1}_{2,0}I^{1,0}_{1,1}\left[I^{1,0}_{0,1}\right]^{n-4}$	0	0	0	$8n-24$	1
(b)6	$I^{0,0}_{2,1}I^{0,2}_{2,0}I^{0,0}_{1,2}I^{1,0}_{0,2}\left[I^{1,0}_{0,1}\right]^{n-4}$	0	0	0	$4n-12$	2
(c)1	$I^{2,1}_{1,2}\left[I^{1,0}_{0,1}\right]^{n-1}$	$0=4-4$	4	4	4	0
(c)2	$I^{1,1}_{1,2}I^{0,1}_{1,1}\left[I^{1,0}_{0,1}\right]^{n-2}$	0	$8=16-8$	16	16	0
(c)3	$I^{1,0}_{1,1}I^{0,1}_{1,1}I^{1,1}_{1,1}\left[I^{1,0}_{0,1}\right]^{n-3}$	0	0	8	8	0
(c)4	$\left[I^{1,0}_{1,1}\right]^2 I^{1,0}_{2,1}\left[I^{1,0}_{0,1}\right]^{n-3}$	0	0	8	8	0
(c)5	$I^{0,0}_{2,1}I^{2,0}_{1,2}\left[I^{1,0}_{0,1}\right]^{n-2}$	0	$0=8-8$	8	8	1
(c)6	$I^{0,0}_{2,1}I^{1,0}_{1,1}I^{1,1}_{2,0}\left[I^{1,0}_{0,1}\right]^{n-3}$	0	0	$8=16-8$	16	1
(c)7	$I^{0,0}_{1,2}I^{0,0}_{2,1}I^{0,2}_{2,0}\left[I^{1,0}_{0,1}\right]^{n-3}$	0	0	$0=4-4$	4	2

Scatterers on which one given amplitude scatters twice are thus, momentarily, not counted as new scatterers. Looking at Fig. 7, m equals the total number of scatterers minus the number of scatterers indicated with curved lines. After this resummation we find the important result that each class of "long range" terms vanishes for m not equal to 2. Denoting the terms of Fig. 7, respectively, by R_a, R_b, and R_c we find $R_a = R_b = R_c = 0$, if $m > 2$. If $m = 2$, the classes cancel against each other, since we then obtain $R_a = R_b = -R_c/2 = \frac{\ell^4}{4k^4}A_1^2$. This implies

$$R_a + R_b + R_c = 0. \tag{62}$$

We have thus shown that the long range diagrams for an infinite system cancel and thus cause no divergency after integration over $\mathbf{q}$. It is essential that the degeneracy of the low order contributions be counted properly.

Another, more standard way to verify the important cancellation is the following. Recall that we look at a bulk situation with fixed internal momentum $\mathbf{q}$, while the external momenta are put equal to zero. Beyond the diffusion approximation an internal diffuson is given by Eq. (61). We also need the Hikami boxes beyond the diffusion approximation. It holds that

$$H_4(\mathbf{q},0,-\mathbf{q},0) = I_{11}^{11}(q) + \frac{4\pi}{\ell}\left\{I_{11}^{10}(q)\right\}^2 + \frac{4\pi}{\ell}\left\{I_{11}^{01}(q)\right\}^2. \tag{63}$$

Inserting the values from Table I and doing similar but longer calculations for two other vertices we find

$$H_4(0,\mathbf{q},0,-\mathbf{q}) = 2H_4(\mathbf{q},-\mathbf{q},0,0) = \frac{\ell^3}{8\pi k^2}A_1(1-A_1), \tag{64a}$$

$$H_6(0,0,\mathbf{q},0,0,-\mathbf{q}) = \frac{\ell^5}{16\pi k^4}A_1(1-A_1)(1-3A_1). \tag{64b}$$

Now the long range diagrams of Fig. 2 can be evaluated. For the internal part one has at fixed $\mathbf{q}$

$$2H_4(\mathbf{q},0,-\mathbf{q},0)^2\mathcal{L}_{\rm int}^2(q) + 4H_4(\mathbf{q},-\mathbf{q},0,0)^2\mathcal{L}_{\rm int}^2(q) + 2H_6(\mathbf{q},0,0,-\mathbf{q},0,0)\mathcal{L}_{\rm int}(q) = \frac{\ell^4}{4k^4}\{2A_1^2 + A_1^2 + 2A_1(1-3A_1)\} = \frac{\ell^4}{4k^4}(2A_1 - 3A_1^2). \tag{65}$$

It is essential that the denominators $1 - A_1$ have disappeared from this expression. As mentioned, it means that all high order terms cancel, allowing a cancellation of the remainder by low order contributions. From Table II it is seen that we have overcounted six types of low order terms. The correction to be subtracted is

$$\frac{4\pi}{\ell}\left\{4\frac{\ell^5}{32\pi k^4}(A_1+A_2+A_3)\right\} + \left(\frac{4\pi}{\ell}\right)^2\left\{\left(\frac{\ell^3}{8\pi k^2}A_1\right)^2 + 8\frac{-i\ell^4}{32\pi k^3}(2A_1+A_2)\frac{-i\ell^2}{8\pi k}A_1 + 8\frac{i\ell^2}{8\pi k}\frac{i\ell^4}{32\pi k^3}(A_2+2A_3)\right\} + \left(\frac{4\pi}{\ell}\right)^3\left\{8\frac{i\ell^2}{8\pi k}\frac{i\ell^2}{8\pi k}A_1\frac{-\ell^3}{16\pi k^2}A_2 + 4\frac{-i\ell^2}{8\pi k}\frac{i\ell^2}{8\pi k}\frac{\ell^3}{8\pi k^2}A_3\right\} = \frac{\ell^4}{4k^4}(2A_1 - 3A_1^2). \tag{66}$$

It indeed exactly cancels expression (65), which arose as a remainder of the long range terms.

From the results of the present section one may be tempted to conclude that the long range diagrams do not lead to divergencies if the correct degeneracies of the low order terms are properly taken into account. Though this conclusion is correct, it is too early to draw it, since we show in the next parts that some further complications arise.

B. Extra short distance contributions

Unfortunately, we have not yet finished with the calculation as other terms are also of leading order at short distances. First, diagrams with a different topology also occur. There are five new diagrams, all with two scatterers; see Fig. 8. They can be looked upon as diagrams from the set of Fig. 7(a), but without any scatterers in the ladders.

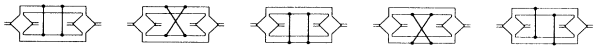

FIG. 8. Leading diagrams with topologies not yet contained in the long range diagrams. They all contain two scatterers.

Second, diagrams can have more than one configuration for a resonant arrangement of the momenta, i.e., several configurations can be leading. The most important contribution to the integral (59) arises if the *amplitude* loop momentum $\mathbf{p}$ is close to the wave vector $|\mathbf{p}| = k$. With more loops present it is sometimes possible to find more than one choice for the momenta of the amplitude propagators. This is illustrated in Fig. 9, where the diagram of Fig. 7(a)1 is repeated. The expression for the shown diagram has contributions from three different poles. The first arrangement of the momenta is dominant for any number of scatterers; this one is part of the set of long range diagrams for any number of scat-

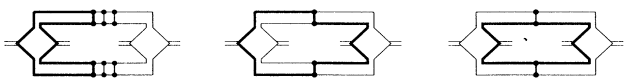

FIG. 9. Different choices for the loop momenta, all yielding leading contributions; thick and thin lines depict different large momenta, both with length k. The first diagram is leading for any number of scatterers. When only two scatterers occur the other two diagrams are also leading.

terers. The two configurations on the right give an extra leading contribution. This only occurs with two scatterers present; with more scatterers the two diagrams on the right become subleading, and only the left diagram remains. Apart from this diagram, the same thing occurs for the diagrams of Fig. 7(c)1 and Fig. 7(c)2 also with two scatterers, and for the diagram Fig. 7(c)6 with three scatterers.

Also the diagrams of Fig. 8 have more than one pole: The four left diagrams of Fig. 8 have two resonant momenta configurations and the right one has three. We sum all the contributions thus found (41 in total) and denote them as S_n for n scatterers. They are only nonzero for diagrams with two or three scatterers, and read

$$S_2=\left(\frac{4\pi}{\ell}\right)^2\left[5(I^{1,1}_{1,1})^2+8I^{1,1}_{1,1}I^{0,1}_{1,2}+12(I^{0,1}_{1,2})^2+8I^{0,1}_{1,1}I^{1,1}_{1,2}\right]$$
$$=\frac{-\ell^4}{2k^4}A_1A_2, \tag{67a}$$

$$S_3=8\left(\frac{4\pi}{\ell}\right)^3 I^{0,1}_{1,1}I^{0,2}_{1,1}I^{0,0}_{1,2}=\frac{\ell^4}{2k^4}A_1A_2. \tag{67b}$$

One sees that these special contributions cancel.

C. Interference vertices without partner exchange

Apart from the diagrams generated by the Kadanoff-Baym approach, we found another class of leading long range diagrams when we generated the diagrams by computer. In these diagrams the two diffusons have two scatterers in common, but no amplitude is exchanged. They either have one internal diffuson (see Fig. 10) or two (see Fig. 11). These diagrams are actually of similar type as Fig. 2. The diagrams with one internal diffuson are analogous to Fig. 2(c)i, while the ones with two internal diffusons are analogous to Figs. 2(a)i and 2(b)i. The equivalents of Figs. 2(a)ii, 2(b)ii, and 2(c)ii also occur. The important difference with the previous diagrams, though, is that at the interference vertices no amplitudes are exchanged. In this respect they differ qualitatively from Hikami boxes, where partner exchange does occur. Explicit calculation shows that these terms cancel at both zero and nonzero external momentum; this was also already noted by Kane, Serota, and Lee [23] [see their Fig. 5(c)]. These classes of diagrams can thus be fully neglected. This cancellation is due to time-reversal invariance. Apart from these two classes, the Kadanoff-Baym approach, using (55), generates all presented diagrams as we checked with the computer program. The generating functional for the extra diagrams of Fig. 10 is drawn in Fig. 12.

In conclusion, the analysis of this section shows that

FIG. 10. Leading diagrams without amplitude exchange with one internal diffuson. The two drawn diagrams cancel against each other. All diagrams of this class cancel.

FIG. 11. Leading diagrams without amplitude exchange with two internal diffusons. The two drawn diagrams cancel against each other. All diagrams of this class cancel.

when the external momenta vanish all leading terms cancel at fixed value of the internal momentum. Upon integration over the loop momentum one still has a zero and, in particular, not a divergent contribution. For an infinite system the theory is thus well behaved at short distances. The divergence has canceled in a careful study of the short distance process; renormalization, as known from field theories, was not needed.

VII. APPLICATION OF CONDUCTANCE FLUCTUATIONS TO OPTICAL SYSTEMS

We have now seen that in infinite systems all divergent terms cancel. In realistic systems, such as a slab, the same diagrams describe the relevant physics. They have to be evaluated with appropriate diffuson propagators. Generally they can be written as the bulk term with additional mirror terms. For a slab they were given in Sec. II. Knowing that the short distance behavior is regular, we can self-consistently consider all scattering diagrams in the diffusion approximation. For the long range diagrams this was done already in Sec. IV, where all long range contributions were evaluated. The discussion of the preceding section has shown that the only new effect comes from the subtraction of Eq. (66). In the diffusion limit for a quasi-one-dimensional system at fixed transversal momentum Q, it results in a contact term, labeled F_d:

$$F_d(M)=\int dz\mathcal{L}^2_{\rm in}(z)\int_{-\infty}^{\infty}\frac{dq_z}{2\pi}\frac{\ell^4}{4k^4}\mathcal{L}^2_{\rm out}(z)$$
$$=\frac{\ell^4}{4k^4}\delta(0)\int dz\mathcal{L}^2_{\rm in}(z)\mathcal{L}^2_{\rm out}(z). \tag{68}$$

This indeed cancels exactly the leading divergency that remained in Eq. (49) for the sum of F_a, F_b, and F_c. The milder divergency present in the individual terms F_a, F_b, and F_c in two and three dimensions canceled already by summing them. Diagrammatically this can be seen as follows. The diagrams responsible for the latter divergence contain one internal diffuson [such as in Fig. 2(c)]. For these diagrams one does not have the complications of the preceding section; double counting corrections, different resonant momentum configurations, and extra diagrams are absent. This was confirmed by our computer gener-

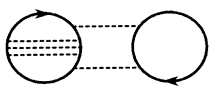

FIG. 12. The generating functional that has to be included in the Kadanoff-Baym approach to generate the diagrams of Fig. 10.

ated diagrams. The only contributions which remain in (49) are thus the double z integrals. This finite remainder of our theory yields the sought conductance fluctuations. We thus obtain, with again $h_4 = \ell^5/(48\pi k^2)$,

$$F(Q,\kappa,\Omega) = F_a(M) + F_b(M) + F_c(M) + F_d(M) \tag{69a}$$

$$= 4h_4^2 \int\int dz\, dz'\, \mathcal{L}_{\rm int}(z,z';M)\mathcal{L}_{\rm int}(z,z';M^*)\,\left[\mathcal{L}'^2_{\rm in}(z)\mathcal{L}'^2_{\rm out}(z') + \mathcal{L}'_{\rm in}(z)\mathcal{L}'_{\rm out}(z)\mathcal{L}'_{\rm in}(z')\mathcal{L}'_{\rm out}(z')\right]$$

$$+\frac{1}{2}h_4^2 \int\int dz\, dz'\,\left[\mathcal{L}^2_{\rm int}(z,z';M) + \mathcal{L}^2_{\rm int}(z,z';M^*)\right]\frac{d^2}{dz^2}\left[\mathcal{L}_{\rm in}(z)\mathcal{L}_{\rm out}(z)\right]\frac{d^2}{dz'^2}\left[\mathcal{L}_{\rm in}(z')\mathcal{L}_{\rm out}(z')\right], \tag{69b}$$

in which again $M^2 = Q^2 + \kappa^2 + i\Omega$. This equation is the central result of the present paper. The upper line of (69b) corresponds to the diagrams of Fig. 2(a), whereas the lower line corresponds to the diagrams of Fig. 2(b). Note that only derivatives of external diffusons are present. As compared to the first line, extra terms are present in the second one. According to (32) we have

$$\frac{d^2}{dz^2}\left[\mathcal{L}_{\rm in}(z)\mathcal{L}_{\rm out}(z)\right] = 2\mathcal{L}'_{\rm in}(z)\mathcal{L}'_{\rm out}(z) + 2\kappa^2\mathcal{L}_{\rm in}(z)\mathcal{L}_{\rm out}(z). \tag{70}$$

The κ terms are extra terms arising when absorption is present. Finally, with Eq. (38c) the value at vanishing transversal momentum gives the variance of the conductance in one dimension, and integration over the transversal momentum yields the correlation in two and three dimensions.

Using the general result of (69) and (38c) various cases are considered by inserting the diffusons derived in Sec. II. First consider the case of fully transmitting surfaces; if we neglect absorption and frequency differences this gives

$$F(Q) = \frac{3}{2}\frac{2 + 2Q^2L^2 - 2\cosh 2QL + QL\sinh 2QL}{Q^4L^4\sinh^2 QL}, \tag{71}$$

which decays for large Q as Q^{-3}. In this case we recover

$$\langle T^2\rangle_c = \begin{cases} \frac{2}{15} \approx 0.133, & \text{quasi 1D} \quad (72)\\ \frac{3}{\pi^3}\zeta(3)\frac{W}{L} \approx 0.116\frac{W}{L}, & \text{quasi 2D} \quad (73)\\ \frac{1}{2\pi}\frac{W^2}{L^2} \approx 0.159\frac{W^2}{L^2}, & \text{3D}, \quad (74)\end{cases}$$

in which ζ is Riemann's zeta function. These are well known results [4]. We determine also the frequency dependency of the correlation; this is important as it determines the frequency range of the light needed to see the fluctuations. Taking the frequency dependency into account we obtain

$$F(Q,\omega) = \frac{4\left(M^{*2} - M^2 + M^2M^*L\coth M^*L - M^{*2}ML\coth ML\right)}{L^4M^2M^{*2}(M^2 - M^{*2})}$$

$$+\mathrm{Re}\frac{2 + 2M^2L^2 - 2\cosh 2ML + ML\sinh 2ML}{2M^4L^4\sinh^2 ML}. \tag{75}$$

The correlation decays for large frequency differences as $\Omega^{2-d/2}$, as was stated by Lee, Stone, and Fukuyama [4].

We were unable to perform the double integral over the position analytically in the presence of absorption. In Figs. 13, 14, and 15 we show the one-, two-, and three-dimensional correlation functions for various values of the absorption. It is seen that especially the top of the correlation is reduced due to absorption.

Next we applied our theory to the case of partial reflection at the surfaces of the sample. We assume an index of refraction $m = \sqrt{\epsilon_0/\epsilon_1} \neq 1$. For our purpose the internal reflections are coded in only one parameter, the injection depth z_0; see (18), (26), and (35). For optically thick samples the correlations are now determined by z_0/L. It is physically clear that the internal reflections lead to a less steep diffuse intensity in the sample as a function of the depth. The fluctuations are proportional to the space derivatives and are thus reduced. The results are presented in Figs. 16–18 where the correlation function is plotted for various values of the ratio between extrapolation length and sample thickness. One sees that

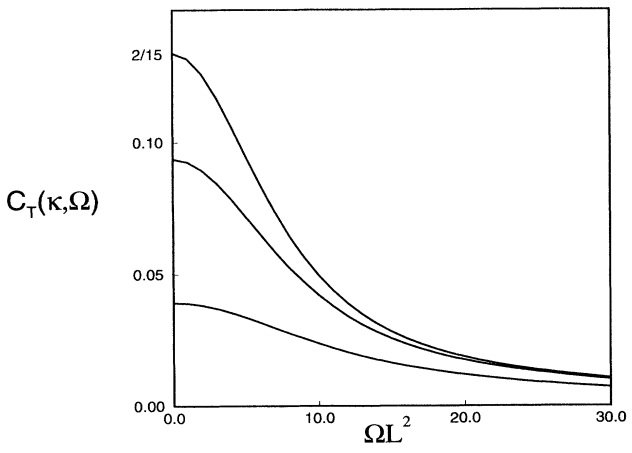

FIG. 13. The correlation of the conductance as a function of the frequency for various absorption strengths in one dimension without internal reflection. From upper to lower curve: no absorption ($\kappa = 0$), $\kappa = 1/L$, and $\kappa = 2/L$.

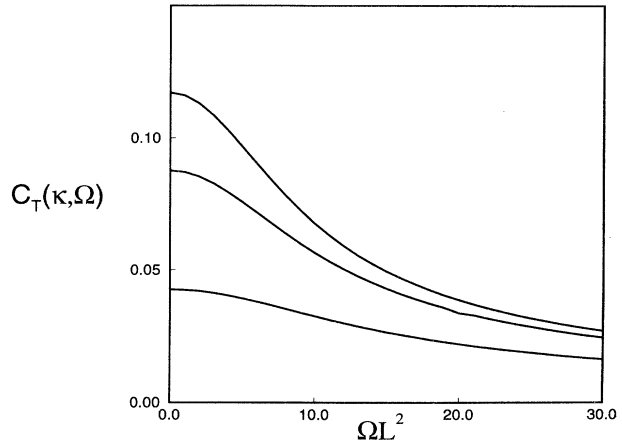

FIG. 14. The correlation of the conductance as a function of the frequency for various absorption strengths in a two-dimensional slab without internal reflection. From upper to lower curve: $\kappa = 0$, $\kappa = 1/L$, and $\kappa = 2/L$.

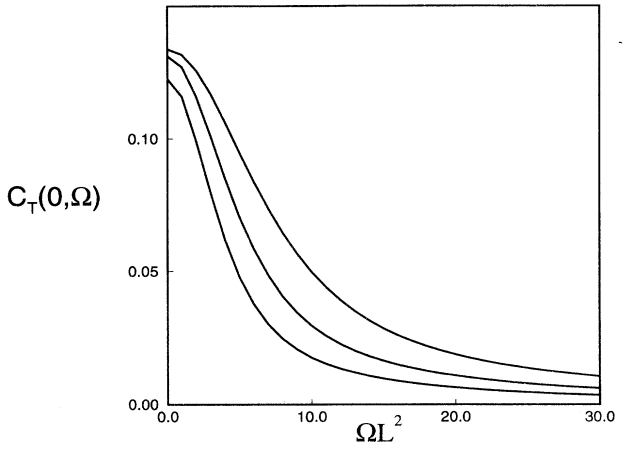

FIG. 16. The influence of internal reflection on the one-dimensional frequency correlation. With $z_0 = 0$, $L/10, L/5$ (upper, middle, lower curve); no absorption. Also here the fluctuations are reduced.

already for small ratios of z_0/L the correlation is significantly lower than without surface internal reflection. It is seen that neither the variance (the value at vanishing Ω) nor the form of the correlations is universal; they are sensitive to absorption and internal reflections.

VIII. DISCUSSION AND OUTLOOK

The universal conductance fluctuations (UCF) of mesoscopic electronic systems have a direct counterpart in other mesoscopic systems with multiply scattered classical waves. The corresponding average normalized correlation function is C_3. It is known that a naive calculation of this object in the Landauer approach is plagued with short distance divergencies. In this work we have presented a detailed diagrammatic approach to the calcula-

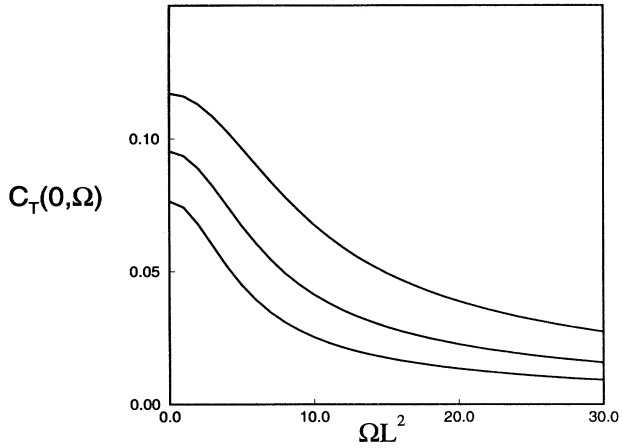

FIG. 17. Influence of internal reflection on the frequency correlation in 2D; $z_0 = 0, L/10, L/5$ (upper, middle, lower curve); no absorption.

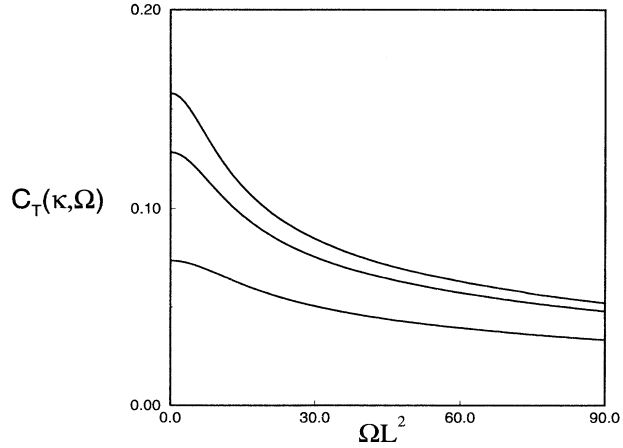

FIG. 15. The conductance correlation function versus the frequency difference for various absorption strengths in a three-dimensional slab without internal reflection. From upper to lower curve: $\kappa = 0$, $\kappa = 1/L$, and $\kappa = 2/L$.

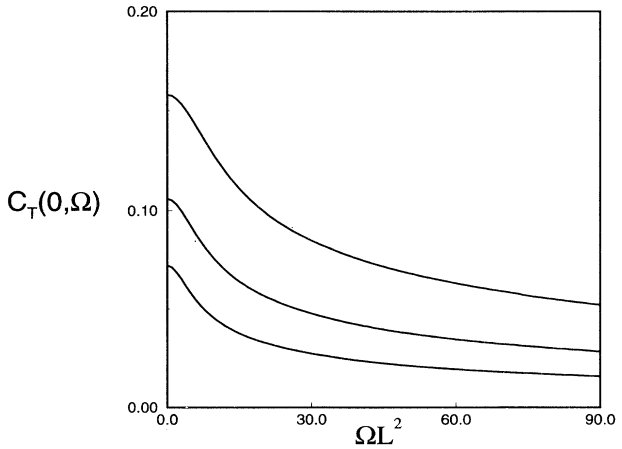

FIG. 18. Influence of internal reflection on the frequency correlation in 3D; $z_0 = 0, L/10, L/5$ (upper, middle, lower curve); no absorption.

tion of the C_3 correlation function. We first evaluated the leading long range diagrams. As expected, each diagram, but also their sum, contains a short distance divergency. Also a subleading divergency occurs, but for a slab geometry is was found to cancel automatically. The study of the cancellation of the leading divergency then was the main theme of the paper. Consistency of the approach requires finding extra contributions that exactly cancel the already determined divergency, and therefore serves as proof that the set of long range diagrams exhausts all of them.

We developed a diagrammatic method that systematically generates all leading scattering diagrams. This set was checked by computer. A large number of diagrams had to be considered in detail. We summed these diagrams for an infinite system at fixed value of the loop momentum. It was seen that also beyond the diffusion approximation the action of Hikami boxes on the long range propagators is to eliminate the long range terms, and leave only some low order contributions. Moreover, some low order terms of diagrams with diffusons have a lower degeneracy than their higher order equivalents. Taking this into account led exactly to a cancellation of all terms in an infinite system. Next we discussed that some extra classes of leading diagrams occur, but they all add up to zero. Thus in an infinite system all diagrams cancel, so that, in particular, no short range divergency occurs. All short range contributions could be coded in a contact term (68). It would be interesting to investigate how it is derived in a nonlinear σ-model formulation of the theory, possibly along the lines of Serota, Esposito, and Ma [39].

Subsequently the theory was applied to systems of finite size. Here the short distance divergencies cancel as well, because the large scale geometry of the system does not have influence on short range effects. The final result is nonzero as it describes the correlation function in terms of derivatives of external diffusion propagators of the geometry considered; such terms have no meaning in an infinite system.

Our central result for the correlation function of the conductance is given in (69). It is obtained by adding the result of the long range diagrams (49) and the contact term (68). When there is no absorption, agreement is found with the result of Kane, Serota, and Lee [23]. All external diffusons are differentiated once. When absorption is present, however, their approach is no longer valid. We found that extra terms appear where some external diffusons are differentiated twice or are proportional to κ^2; see (70).

We have applied the results to realistic optical systems. The frequency dependent C_3 correlation function was calculated for the case where a diffuse incoming beam is used and all outgoing intensity is collected. It was seen that both absorption and internal reflections decrease the correlations by a considerable amount. This is important for a quantitative analysis of experimental data.

Electromagnetic measurements that involve the C_3 correlation have been reported by Garcia and Genack [40]. These authors were able to describe the data of their infrared experiments by adding the C_1, C_2, and C_3 contributions, but they incorrectly assumed that C_3 is frequency independent. The experimental investigation of optical universal conductance fluctuations is known to be very difficult. One problem is that if the incoming beam has to be diffusive, it will have a low intensity.

We propose here a different way to measure the same interference effect. Consider a laser beam coming in in a given direction a and measure the frequency dependent total transmission. Such can be done using an integrating sphere [9]. Then repeat the measurement for a very different incoming direction c. Each of these two signals will exhibit the large C_2 correlation function [9]. However, when the directions a and c are not close to each other, the C_2 will not contribute to the *cross correlation.* The cross correlation of the total transmission is much smaller than the autocorrelations; it just represents the typical term of the UCF in (39). As this cross correlation is of relative order $1/g^2$, it is of the same order of magnitude as the third cumulant of the total transmission. A very precise measurement of that quantity was carried out by de Boer, van Albada, and Lagendijk, and reported in collaboration with two of us [10]. It may therefore be expected that it is just possible to measure C_3, and thus essentially the UCF, with visible light.

ACKNOWLEDGMENTS

M.v.R. thanks A. Genack, J. Hoogland, J. F. de Boer, and H.J. Kop for discussions. Th.M.N. thanks P. A. Lee, B. L. Altshuler, I. V. Lerner, and Shechao Feng for discussions. R.V. kindly acknowledges helpful discussions with G. Schön on the theory presented in Sec. V. The research of Th.M.N. was supported by the Royal Netherlands Academy of Arts and Sciences (KNAW) and was also sponsored by NATO (Grant No. CGR 921399). The research of R.V. was supported by the Stichting voor Fundamenteel Onderzoek der Materie (FOM).

[1] C. P. Umbach, S. Washburn, R. B. Laibowitz, and R. A. Webb, Phys. Rev. B **30**, 4048 (1984).

[2] B. L. Altshuler, Pis'ma Zh. Eksp. Teor. Fiz. **41**, 530 (1985) [JETP Lett. **41**, 649 (1985)].

[3] P. A. Lee and A. D. Stone, Phys. Rev. Lett. **55**, 1622 (1985).

[4] P. A. Lee, A. D. Stone, and H. Fukuyama, Phys. Rev. B **35**, 1039 (1987).

[5] *Mesoscopic Phenomena in Solids*, edited by B. L. Altshuler, P. A. Lee, and R. A. Webb (North-Holland, Amsterdam, 1991), Vol. 30.

[6] W. van Haeringen and D. Lenstra, *Analogies in Optics and Micro Electronics* (Kluwer Academic, Haarlem, 1990).

[7] M. P. van Albada and A. Lagendijk, Phys. Rev. Lett. **55**, 2692 (1985).

[8] M. P. van Albada, J. F. de Boer, and A. Lagendijk, Phys. Rev. Lett. **64**, 2787 (1990).

[9] J. F. de Boer, M. P. van Albada, and A. Lagendijk, Phys. Rev. B **45**, 658 (1992).
[10] J. F. de Boer *et al.*, Phys. Rev. Lett. **73**, 2567 (1994).
[11] R. Berkovits and S. Feng, Phys. Rep. **238**, 135 (1994).
[12] S. Feng, C. Kane, P. Lee, and A. D. Stone, Phys. Rev. Lett. **61**, 834 (1988).
[13] N. Garcia and A. Z. Genack, Phys. Rev. Lett. **63**, 1678 (1989).
[14] A. Z. Genack, N. Garcia, and W. Polkosnik, Phys. Rev. Lett. **65**, 2129 (1990).
[15] M. J. Stephen, in *Mesoscopic Phenomena in Solids* [5], p. 81.
[16] J. X. Zhu, D. J. Pine, and D. A. Weitz, Phys. Rev. A **44**, 3948 (1991).
[17] A. A. Lisyansky and D. Livdan, Phys. Lett. A **170**, 53 (1992).
[18] M. C. W. van Rossum and Th. M. Nieuwenhuizen, Phys. Lett. A **177**, 452 (1993).
[19] R. Landauer, Z. Phys. B **21**, 247 (1975).
[20] M. Büttiker, Phys. Rev. Lett. **57**, 1761 (1986).
[21] D. S. Fisher and P. A. Lee, Phys. Rev. B **23**, 6851 (1981).
[22] M. Janßen, Solid State Commun. **79**, 1073 (1991).
[23] C. L. Kane, R. A. Serota, and P. A. Lee, Phys. Rev. B **37**, 6701 (1988).
[24] B. L. Altshuler, V. E. Kravtsov, and I. V. Lerner, in *Mesoscopic Phenomena in Solids* [5], p. 449.
[25] Th. M. Nieuwenhuizen and M. C. W. van Rossum, Phys. Rev. Lett. **74**, 2674 (1994).
[26] Th. M. Nieuwenhuizen and J. M. Luck, Phys. Rev. E **48**, 569 (1993).
[27] H. C. van de Hulst, *Multiple Light Scattering* (Academic, New York, 1980), Vols. 1 and 2.
[28] Th. M. Nieuwenhuizen, A. Lagendijk, and B. A. van Tiggelen, Phys. Lett. A **169**, 191 (1992).
[29] Th. M. Nieuwenhuizen and M. C. W. van Rossum, Phys. Lett. A **177**, 102 (1993).
[30] M. P. van Albada, B. A. van Tiggelen, A. Lagendijk, and A. Tip, Phys. Rev. Lett. **66**, 3132 (1991).
[31] L. P. Gor'kov, A. I. Larkin, and D. Khmel'nitskii, Pis'ma Zh. Eksp. Teor. Fiz. **30**, 248 (1979) [JETP Lett. **30**, 228 (1979)].
[32] S. Hikami, Phys. Rev. B **24**, 2671 (1981).
[33] M. C. W. van Rossum, J. F. de Boer, and Th. M. Nieuwenhuizen Phys. Rev. E (to be published).
[34] G. Baym and L. Kadanoff, Phys. Rev. **124**, 287 (1961).
[35] G. Baym, Phys. Rev. **127**, 1391 (1962).
[36] G. S. Uhrig (private communication).
[37] K. N. Efetov, Adv. Phys. **32**, 53 (1983).
[38] R. Vlaming (unpublished).
[39] R. A. Serota, F. P. Esposito, and M. Ma, Phys. Rev. B **39**, 2952 (1989).
[40] N. Garcia and A. Z. Genack, Phys. Rev. Lett. **66**, 1850 (1991).